

Local paths to global coherence: Cutting networks down to size

Yu Hu¹, James Trousdale², Krešimir Josić^{†2,3}, and Eric Shea-Brown^{†1,4,5}

¹Department of Applied Mathematics, University of Washington, Seattle, WA 98195

²Department of Mathematics, University of Houston, Houston, TX 77204-5001

³Department of Biology and Biochemistry, University of Houston, Houston, TX 77204-5001

⁴Program in Neurobiology and Behavior, University of Washington, Seattle, WA 98195

⁵Department of Physiology and Biophysics, University of Washington, Seattle, WA 98195

June 21, 2022

Abstract

How does connectivity impact network dynamics? We address this question by linking network characteristics on two scales. On the global scale we consider the coherence of overall network dynamics. We show that such global coherence in *activity* can often be predicted from the local *structure* of the network. To characterize local network structure we use “motif cumulants,” a measure of the deviation of pathway counts from those expected in a minimal probabilistic network model.

Our contributions are threefold: First, we give a new combinatorial formulation of motif cumulants that connects with the allied concept in probability theory. Second, we show that the link between global network dynamics and local network architecture is strongly affected by heterogeneity in network connectivity. However, we introduce a network-partitioning method that recovers a tight relationship between architecture and dynamics. Third, for a particular set of models we generalize the underlying theory to treat dynamical coherence at arbitrary orders (i.e. triplet correlations, and beyond), and show that at any order only a highly restricted set of motifs impact dynamical correlations.

[†]These authors contributed equally.

I Introduction

From genetics to neuroscience to the social world, networks of stochastic dynamical systems are ubiquitous. The architecture of these networks is complex: irregular but far from random, with an unexpected prevalence of specific connection features [1, 2, 3, 4, 5]. At the same time, networks produce complex patterns of collective dynamics [6, 7, 8]. Here we explore the links between these two phenomena and provide general principles that relate network architecture to collective dynamics.

How can the collective dynamics of a network be usefully quantified? The joint activity of pairs and groups of nodes is frequently described using pairwise and higher-order correlations (coherence) [9, 10, 11, 12, 13]. Specifically, consider the time dependent activity of a node $x_i(t)$. Then, the pairwise correlation is $\text{cov}(x_i(t), x_j(t)) = \mathbf{E}\{x_i(t)x_j(t)\} - \mathbf{E}\{x_i(t)\}\mathbf{E}\{x_j(t)\}$. One can also compare activities separated by a certain delay, $\text{cov}(x_i(t), x_j(t+\tau))$, and thus acquire the correlation function (of τ). Another useful generalization is to higher order correlations that consider three or more nodes at a time.

But what do such measures of coherence tell us? Clearly, a high average correlation (across all node pairs) reflects the tendency to synchronize. In some settings, this global synchrony is what matters for how strongly a network will “cooperate” to influence a system downstream [14, 15, 16, 17, 18]. Beyond the strength of downstream interactions, synchrony can also impact how information is encoded in a network. This has been widely studied in the neural networks of sensory pathways, which encode signals from the external world; here, synchronous fluctuations can either serve as a separate “channel” to encode these signals, or can modulate the amount of information that network responses can carry by shaping their overall signal-to-noise ratios [19, 20, 21, 22, 23, 24].

Thus motivated, we turn to the question of relating coherent network dynamics to network connectivity structures – described by a directed graph with weighted edges specifying interactions between nodes. Despite significant progress [9, 25, 26, 10, 11], this problem remains a challenge. Our approach is to identify the key *local* connectivity features of a complex network that predict *global* levels of correlation — that is, the averaged correlation across all nodes in the network. We characterize local connectivity using specific pathways between subsets of nodes, or motifs. Formally, motifs are certain connectivity patterns (usually smaller graphs) that can occur, possibly multiple times, in the graph of the network. Several examples of such network motifs are shown in Fig. 1.

How can motif structure be used to predict network-wide correlation? An approximate expression relating network-wide correlations to the frequency of different types of network motifs has been derived previously [10, 27]. Although this result lead to a number of insights, it is difficult to apply generally due to the combinatorial explosion of motifs that appear in the approximation [10, 27, 28]. It is necessary to measure empirically the frequencies of many different motifs in order to apply the theory. In earlier work we sought to simplify the situation [28]. We first used the frequency of a few, smaller motifs to predict the frequency of larger motifs in the network. As a result we showed that the frequency of a few small motifs alone could predict network-wide correlation — in many cases with a high level of accuracy.

However, three key questions remain unanswered. First, under what conditions can a set of small motifs be used to accurately infer the frequency of large motifs? Second, what features of network connectivity predict higher order correlations? Third, when our earlier methods fail [28] — that is, when the frequency of small motifs alone does not provide accurate information about correlations — is there a way to redefine motifs and still cut the dynamical complexity down to size?

Here we answer these questions. We first summarize, and where necessary reinterpret, our earlier results [28] employing new combinatorial definitions: Borrowing ideas from probability theory we define motif moments and cumulants. This abstract approach both reveals the probabilistic structure of our underlying assumptions and allows us to immediately generalize our theory to link higher order correlations in network dynamics to graphical features described by frequencies of more complex motifs. Intriguingly, only a highly restricted set of motifs at any order enter in expressions for dynamical correlations. We explicitly identify these motifs at every order. Finally, we show that heterogeneity in network connectivity can lead to a failure of our predictive approach. However, even in this case an accurate approximation can be obtained if the network is correctly partitioned, and motif frequencies are measured within and across the partitions.

Our results for coherence at both second and higher orders hold for stochastic networks where node interactions can be described using linear response, including linear SDEs

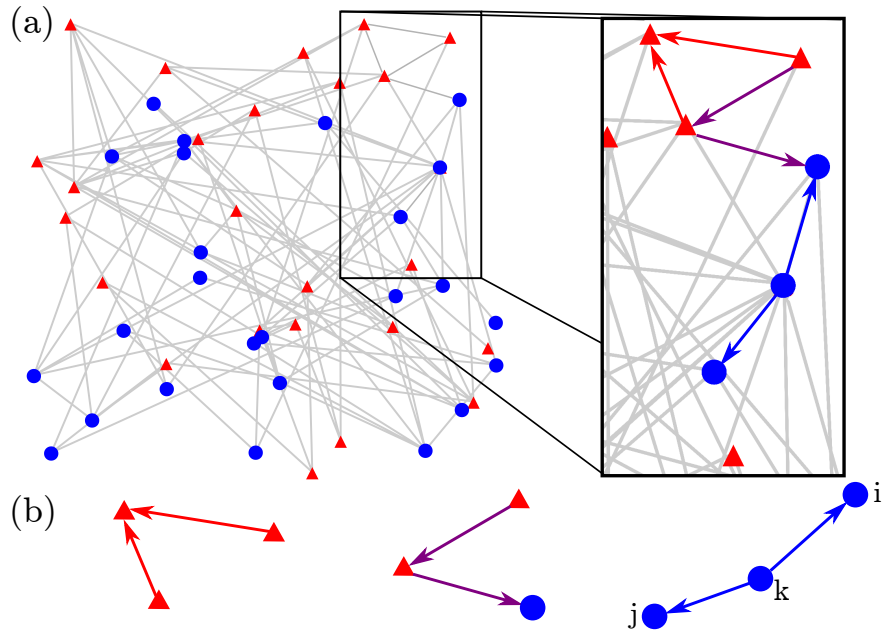


FIG. 1: (a) We consider directed, recurrent, networks within which motifs of different orders, i.e. number of edges, are identified. The inset illustrates how these motifs are embedded in the graph. (b) Left to right: second order converging, chain, and diverging motifs, as highlighted in the inset of (a). Only the latter two contribute to correlations in the path expansion given by Eq. (4).

(Ornstein-Uhlenbeck) and shot noise processes [29] on networks. Moreover, our findings for second (but not higher) order coherence also hold for coupled point process systems; including networks of integrate-and-fire neurons [27], as well as linearly interacting point processes (Hawkes models [30, 10]).

II Network models

Stochastic networks of linearly interacting units can generally be described using

$$y_i(t) = x_i(t) + A_i(t) * \sum_j \mathbf{W}_{ij} y_j(t). \quad (1)$$

Here the activity of the i^{th} node, $y_i(t)$, is perturbed linearly from a (stochastic) baseline $x_i(t)$ by filtered input ($*$ stands for convolution) from the rest of the network. The response of unit i is captured by its linear response function $A_i(t)$, and \mathbf{W}_{ij} is the connection strength of the input from unit j to unit i . We illustrate many of our ideas with a form of the widely used Ornstein-Uhlenbeck (OU) model of biological networks [31, 32, 33, 34] described by Eq. (1). We describe how the OU process can be put into the form of Eq. (1) and provide details about our numerical simulations in Appendix C.

Our goal is to relate network architecture, described by the matrix \mathbf{W} , to coherence in network dynamics. At second order, coherence is measured by the cross-covariance between the activities of nodes i and j as a function of time lag τ , $(\mathbf{C}_y(\tau))_{ij}$ [35]. As computations are simpler in the spectral domain, we first consider the cross-spectra, $\mathbf{S}_y(\omega) = \mathbf{E} [\tilde{\mathbf{y}}\tilde{\mathbf{y}}^T]$ [36], of the processes (\tilde{z} is a complex conjugate, T is a transpose, and bold symbols represent column vectors or matrices). Cross-spectra and cross-covariances are related by the Wiener-Khinchin Theorem, $\mathbf{S}_y(\omega) = \mathcal{F}(\mathbf{C}_y(\tau))$.

For simplicity, we assume that connection weights are uniform, so that $\mathbf{W} = w\mathbf{W}^0$ for an adjacency matrix \mathbf{W}^0 . We also assume that the nodes are homogeneous in their dynamics and response to inputs, so that $A_i(t) = A(t)$, and $x_i(t)$ are i.i.d. processes. These assumptions can be relaxed as explained in [28].

After a Fourier transformation, the matrix form of Eq. (1) is

$$\tilde{\mathbf{y}}(\omega) = \tilde{\mathbf{x}}(\omega) + \tilde{A}(\omega)\mathbf{W}\tilde{\mathbf{y}}(\omega). \quad (2)$$

If the spectral radius $\Psi(\tilde{A}(\omega)\mathbf{W}) < 1$, then Eq. (2) implies $\tilde{\mathbf{y}} = (\mathbf{I} - \tilde{A}\mathbf{W})^{-1}\tilde{\mathbf{x}}$, where \mathbf{I} is the identity matrix. This leads to the following relation between the matrix of cross-spectra, and auto-spectra of the isolated (baseline) nodes,

$$\mathbf{S}_y(\omega) = (\mathbf{I} - \tilde{A}\mathbf{W})^{-1}\mathbf{S}_x(\omega)(\mathbf{I} - \tilde{A}\mathbf{W}^T)^{-1}. \quad (3)$$

This shows how the baseline variability within individual nodes, $\mathbf{S}_x(\omega) = S_x(\omega)\mathbf{I}$, propagates through the network. An analog of Eq. (3) holds for integrate-and-fire neuronal networks and Hawkes processes [30, 27], and our findings about pairwise covariances extend to these systems.

Eq. (3) can be expanded in a series [27, 28, 10],

$$\mathbf{S}_y(\omega)/S_x(\omega) = \sum_{n,m=0}^{\infty} \bar{\tilde{A}}^n \tilde{A}^m \mathbf{W}^n (\mathbf{W}^T)^m. \quad (4)$$

The cross-spectra are normalized by $S_x(\omega)$ to obtain a unitless measure of network coherence, which we can use to approximate average correlation coefficient (see [28]).

As shown by [10, 27], the sum in Eq. (4) represents contributions to the cross spectrum from paths (i.e., motifs) within the network. Fig. 1 shows some example second order motifs. For instance, the second order term $\bar{\tilde{A}}\tilde{A}(\mathbf{W}\mathbf{W}^T)_{ij} = w^2|\tilde{A}|^2 \sum_k \mathbf{W}_{ik}^0 \mathbf{W}_{jk}^0$ counts all contributions to the cross-spectrum of nodes i and j due to common input from nodes k (the rightmost motif in Fig. 1(b)). In general $(\mathbf{W}^n(\mathbf{W}^T)^m)_{ij}$ represents the contribution of (n, m) motifs which consist of two directed chains of length n and m emanating from a single apex and terminating in nodes i and j , respectively. The same node can be visited multiple times, and the $(0, m)$ motif is a chain of length m .

Fig. 2 illustrates such an expansion for two mutually inhibiting nodes (see also [27]). The cross-covariance between the nodes is shown in Fig. 2(a) with contributions of low order motifs in Fig. 2(b). As motif order increases, corresponding contributions decrease in magnitude, but increase in width. The asymmetry of a contribution increases with the asymmetry of the associated motif, *i.e.* the difference between n and m in an (n, m) motif: Compare the contributions of the $(1, 2)$ and $(0, 3)$ motifs. A graphical decomposition of the circuit into the first few (n, m) motifs is shown in the inset of Fig. 2(b). Since the network is recurrent, the expansion in Eq. (4) does not terminate as a node can appear multiple times in a motif.

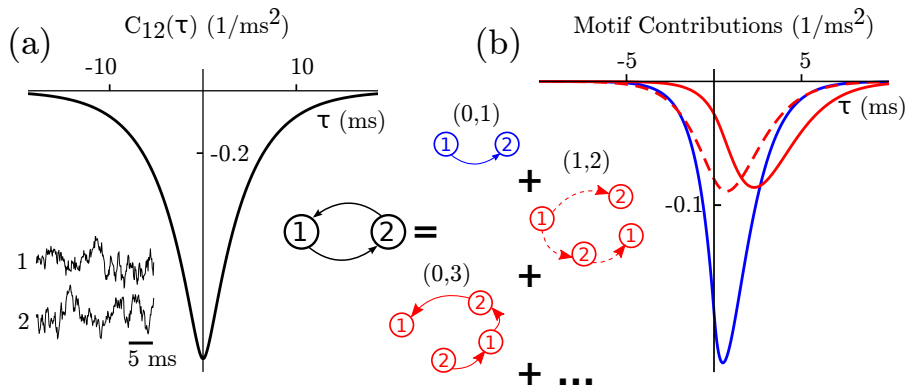


FIG. 2: (a) The cross-correlation function of two mutually inhibiting nodes of Ornstein-Uhlenbeck process; inset shows traces of $y_1(t)$ and $y_2(t)$. (b) Contribution of first- and third-order motifs to the cross-correlation function in (a). (Middle Inset) Diagrammatical expansion of the network showing motifs whose contributions are given, via the same line and color types, in (b).

We include a notation summary in Table I in the Appendix.

III Moments, cumulants, and network-wide coherence

We next relate network coherence and network structure using motif statistics. For concreteness – but without loss of generality [10, 27] – we consider the total covariance between pairs of nodes. This is equivalent to evaluating all spectral quantities at $\omega = 0$, and we indicate this by suppressing dependences on ω . We measure network-wide coherence using the average of this total covariance over all pairs of nodes. As in [10, 28, 27], if we denote by $\langle \mathbf{X} \rangle$ the empirical average of the entries of matrix \mathbf{X} , we obtain from Eq. (4)

$$\langle \mathbf{S}_y \rangle / S_x = \sum_{n,m=0}^{\infty} \tilde{A}^{n+m} \langle \mathbf{W}^n (\mathbf{W}^T)^m \rangle =: \frac{1}{N} \sum_{n,m=0}^{\infty} g^{n+m} \boldsymbol{\mu}_{n,m}, \quad \text{where} \quad g = N \tilde{A} w. \quad (5)$$

Here the *motif moment*, $\boldsymbol{\mu}_{n,m} = \langle \mathbf{W}^{0n} (\mathbf{W}^{0T})^m \rangle / N^{n+m-1}$, is the empirical probability of observing an (n, m) motif in the network [10, 28]. Note that the empirical average is defined over a particular realization of the adjacency matrix \mathbf{W}^0 . We define $\boldsymbol{\mu}_{n,0} = \boldsymbol{\mu}_n$, and let $\boldsymbol{\mu}_{0,0} = 1$. The entire hierarchy of motif moments, $\boldsymbol{\mu}_{n,m}$, needs to be known to evaluate Eq. (5) exactly. In practice, only a subset of $\boldsymbol{\mu}_{n,m}$, up to a certain order $n + m \leq k_{\max}$, is known and can be used with Eq. (5) to approximate network-wide covariance.

Truncating Eq. (5) at some order, yields an approximation of average coherence in terms of motif moments up to that order. However, these approximations can exhibit significant deviations from the true value [28]. Previously, we introduced an alternative, ‘motif resummation approximation’ [28], which provided a series expansion of average coherence in terms of motif *cumulants* (defined below) rather than motif moments. As we show below, truncation of this series at a specified order yielded a different approximation of average coherence. Moreover, this cumulant-based approach improves predictions about dynamical coherence with a given level of information about local network structure.

While we earlier provided a probabilistic interpretation of this approach, a general framework was missing [28]. We next provide such a framework, in particular, by reintroducing the motif cumulants $\boldsymbol{\kappa}_{n,m}$ that first appeared in [28]. We provide a novel definition which clarifies the underlying combinatorial relationship between motif cumulants $\boldsymbol{\kappa}_{n,m}$ and motif moments $\boldsymbol{\mu}_{n,m}$, analogous to that between cumulants and moments of a random variable. Equipped with this new definition, we are able to express dynamical correlations of all orders in terms of motif cumulants (Sec. V).

The construction of motif moments from cumulants is based on a familiar interpretation: estimating the probability of a joint event from the probability of its constituents. Fig. 3(a) demonstrates this for an example motif. Each term in the decomposition of this (2,1) diverging motif arises from a cumulant of smaller or equal order. The first term corresponds to the probability of the motif occurring in a network with edges chosen independently, *i.e.* an Erdős-Rényi network. Subsequent terms give corrections from excess occurrences of second and third order submotifs. Thus, each motif cumulant, $\boldsymbol{\kappa}_{n,m}$, captures “pure” higher order connectivity statistics. Such decomposition can also be expressed in combinatorial form. Let

$\mathcal{C}(n)$ be the set of all compositions (*ordered* partitions) of n . Then

$$\boldsymbol{\mu}_n = \sum_{\{n_1, \dots, n_t\} \in \mathcal{C}(n)} \left(\prod_{i=1}^t \boldsymbol{\kappa}_{n_i} \right) \quad (6)$$

$$\boldsymbol{\mu}_{n,m} = \sum_{\substack{\{n_1, \dots, n_t\} \in \mathcal{C}(n) \\ \{m_1, \dots, m_s\} \in \mathcal{C}(m)}} \left(\prod_{i=2}^t \boldsymbol{\kappa}_{n_i} \right) (\boldsymbol{\kappa}_{n_1, m_1} + \boldsymbol{\kappa}_{n_1} \boldsymbol{\kappa}_{m_1}) \left(\prod_{j=2}^s \boldsymbol{\kappa}_{m_j} \right) \quad (7)$$

In evaluating these terms, we set $(\prod_{i=2}^t \boldsymbol{\kappa}_{n_i}) = 1$ if $t = 1$.

These expressions define $\boldsymbol{\kappa}_{n,m}$ recursively. We note that these are exactly the same quantities expressed in terms of matrix products, Eq. (32) in [28] (see Appendix D).

Using these motif cumulants $\boldsymbol{\kappa}_{n,m}$, one can re-express mean coherence as:

$$\frac{\langle \mathbf{S}_y \rangle}{S_x} = \frac{1}{N} \left(1 - \sum_{n=1}^{\infty} g^n \boldsymbol{\kappa}_n \right)^{-2} \left(1 + \sum_{n,m=1}^{\infty} g^{n+m} \boldsymbol{\kappa}_{n,m} \right). \quad (8)$$

Fig. 3 illustrates how expansions (5) and (8) provide complementary information of about the role of network paths in generating coherent activity. We apply both expansions to three example networks (whose construction and differences will be the topic of later sections). This illustrates a general trend: Truncating Eq. (5), and keeping only terms with $n + m \leq k_{\max}$, approximates the contributions of these (n, m) motifs to the mean dynamical coherence in the network. A similar truncation of Eq. (8) however approximates coherence in terms of contributions of paths of *all* orders. In this latter case, frequencies of motifs of order exceeding k_{\max} are *predicted* from the observed frequencies of motifs of order up to k_{\max} . Fig. 3(c) shows that these predictions are useful: values of correlations based on cumulants converge more quickly than those derived from motif moments. The difference can be explained by looking at the magnitude of the cumulants/moments against the order (Fig. 3(b)). Importantly, cumulants decay much faster than moments in all three cases — hence the increased accuracy of Eq. (8) over Eq. (5) at a given order.

Fig. 3(b) also illustrates that heterogeneity in network architecture can impact how quickly cumulants and moments decay, an observation we will revisit. The networks used in Fig. 3(b) and (c) have a variable degree of *clustering* or “clumping” in network connectivity — we precisely define our graph generation rules below. A greater degree of clustering results in a slower decay of both motif moments and cumulants, and higher order statistics are necessary to accurately describe the structure of these networks. Hence, with more heterogeneity in connections across a network, the frequency of larger, more complex graph motifs has a greater impact on network coherence.

IV Network complexity and subpopulation cumulants

Motif cumulants — via Eq. (8) — provide a way to estimate global dynamical correlation in terms of local network structure. The accuracy of such approximations depends on the

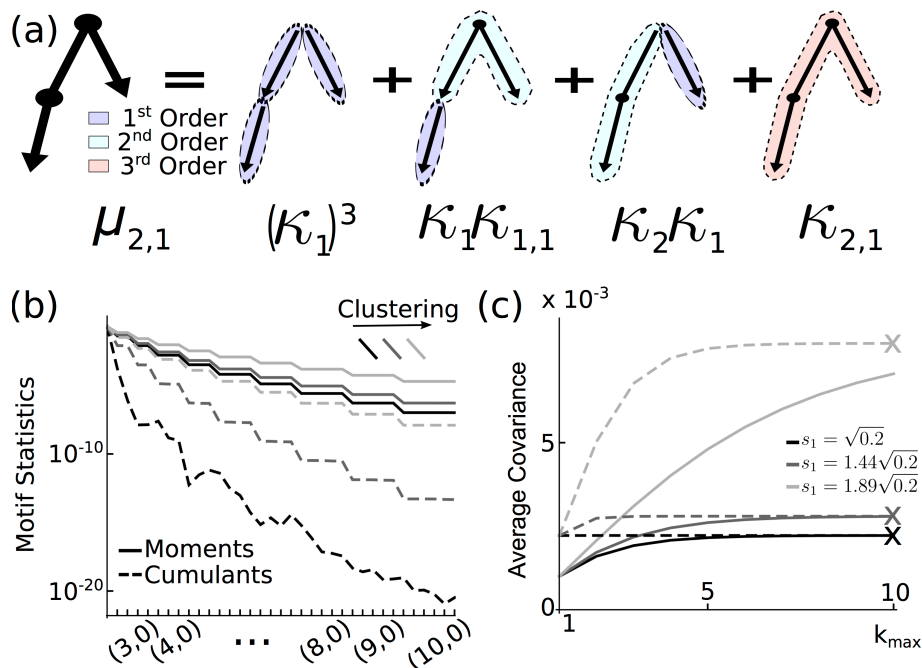


FIG. 3: (a) The probability of observing the motif $(\mu_{2,1})$ decomposed in terms of *motif cumulants* of the graph. (b) The magnitude of motif cumulants (dashed lines) and moments (solid lines) for stochastic block networks with $N = 1000$, $p = 0.2$. Clustering in network connectivity increases from darker to lighter line color (see text for definition of clustering and network structure; precise values as specified in legend of (c)). The (n, m) motifs with $n \geq m$ are listed first by order $n + m$ then arranged by increasing n within the motifs of same order. (c) Approximations of average covariances using motif moments (Eq. (5)) and cumulants (Eq. (8)) truncated at order k_{\max} . Crosses indicate exact values obtained from Eq. (3).

network’s architecture (See Fig. 3). We next highlight the key impact of heterogeneity or clustering in network connectivity on the approximation. We then introduce a partitioning approach, and the allied concept of subpopulation cumulants, which allow us to relate local network structure to dynamics even in heterogeneous networks.

A Heterogeneity in network architecture

As an illustrative example, we consider the two-cluster *stochastic block network model* [37, 38, 39] illustrated in Fig. 1. Such networks are comprised of two subpopulations of size $N/2$ (indicated by circular and triangular nodes), each associated with a constant s_i , $i = 1, 2$. The connection probability between nodes in subpopulation i and j is $p_{ij} = s_i s_j$. With fixed overall connection probability p , the difference between s_1 and s_2 describes the degree of clustering in the network. The case $s_1 = s_2$ corresponds to an Erdős-Rényi network (no clustering), while $s_1 = 2\sqrt{p}$, $s_2 = 0$ implies that only nodes in the first subpopulation are connected (extremal clustering).

We generate three networks with different s_1, s_2 , which are used in Fig. 3(b,c). Comparing pairs of curves (moments or cumulants) with different shades (i.e., different degrees of clustering) reveals the dependence of motif moments and cumulants on graph structure. Motif moments and cumulants (Fig. 3(b)), and their impact on dynamical coherence of motifs of a given order (Fig. 3(c)), are all larger for more heterogeneous, more clustered networks. Moreover, network motifs of increasing order are needed to accurately predict dynamical correlations as clustering increases. Networks generated using the Barabasi-Albert model behave similarly [40], a point we return to below (See also Fig. 7 in the Appendix).

These results agree with intuition. Erdős-Rényi networks have an architecture that is “statistically homogeneous,” as the probability of each link occurring in the network is the same. Thus, the most local network statistic – connection probability – fully determines graph structure and hence levels of dynamical coherence. Similarly, ‘nearly Erdős-Rényi’ networks are without significant graphical heterogeneity, and low order motif cumulants can accurately predict dynamical coherence. On the other hand, in, e.g., highly clustered networks the probability of a path between a set of nodes depends on higher order connectivity statistics. As a result, the frequency of large motifs cannot be obtained accurately from the frequencies of smaller ones. Hence, higher-order motif statistics have a significant impact on dynamical coherence in networks with heterogeneous connectivity.

The necessity of estimating the frequency of higher order motifs could be a significant limitation in applications. In many situations the full connectivity structure of a network is not known, and such global quantities are difficult to estimate. For instance, in the case of biological neuronal networks, the number of neurons which can be simultaneously recorded in order to map out their connectivity is often limited to only a small handful [2, 3]. Moreover, many networks possess additional structure past simple heterogeneities in the graph structure — for instance, neuronal networks may be composed of both excitatory and inhibitory cells. Accounting for such natural subdivisions of the graph can lead to more accurate approximations of dynamical coherence.

B Subpopulation cumulants

We next show how to subdivide a network to tame the effects of heterogeneity in architecture, and re-establish the link between local connectivity and global coherence. Subsets of nodes can be grouped into classes, or subpopulations, that share features of dynamics or connectivity. We focus on the latter possibility, and (once a division is given) characterize each subpopulation with its own motif statistics. Specifically, for b subpopulations, $\boldsymbol{\mu}_{n,m}$ becomes a $b \times b$ matrix of motif moments. Entry p, q of this matrix is the empirical probability of an (n, m) motif with end nodes belonging to populations p and q , respectively. Motif cumulants $\boldsymbol{\kappa}_{n,m}$ are defined by recursive relationships similar to Eqs. (6,7) (See Appendix Eqs. (29, 30)). This distinction of nodes and motifs by population is depicted in Fig. 1, where the color of a node indicates its class. Motifs may involve either nodes of a single class (red and blue edges), or a combination of the two.

How should these population-specific motif cumulants be combined to estimate average correlation? An extension of Eq. (8) for multiple populations developed in [28], and reproduced in Appendix G for completeness, gives average covariances in terms of the matrices $\boldsymbol{\kappa}_{n,m}$ (Eq. (31)). In fact, the two formulae (and the derivations) are very similar once scalar quantities (whole network motif cumulants) are replaced by matrices (consisting of motif cumulants within and across subpopulations). Fig. 4(a) demonstrates this approach with the stochastic block model networks. If nodes are grouped according to the division in the stochastic block network model, first order motif cumulants *alone* perfectly predict average correlations (compare with Fig. 3(b)).

Importantly, the subpopulation approach also works when there is no obvious grouping of nodes. As an example, consider the highly heterogeneous Barábasi-Albert networks. If we order nodes by degree, two subpopulations can be formed from nodes with degrees above and below a given threshold. Fig. 4(b) shows that this approach substantially simplifies the link between network structure and dynamics: if the subpopulations are chosen optimally, covariance in the network dynamics can be accurately predicted using motifs of only order two, while motifs up to order four or five are needed otherwise.

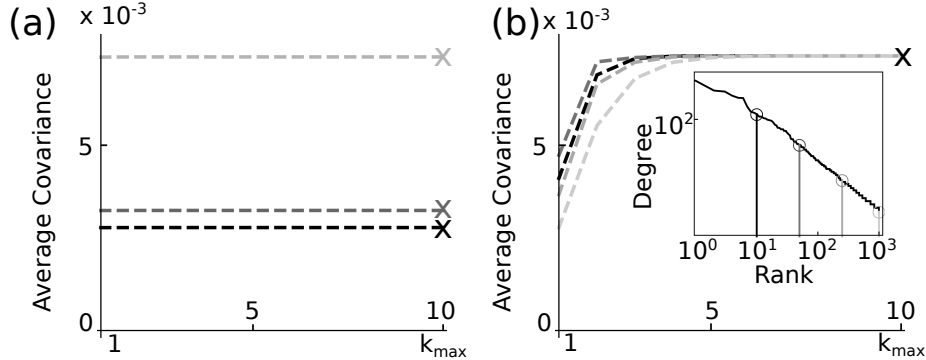


FIG. 4: Approximations of average covariances using the subpopulation cumulant approach, truncating at order k_{\max} . Crosses indicate exact values obtained from Eq. (3). (a) Stochastic block model networks of Fig. 3 (same color scheme) divided into two subpopulations — first order motif cumulants now provide a complete description of the network structure; (b) Barabási-Albert network divided into two subpopulations according to whether the sum of in- and out-degrees of each node lie above or below different thresholds (inset shows cut-off degree ranks (descending)).

C How to partition a network and why it works

In [28], we provided an intuitive argument for why estimates of network-wide covariance converge faster using the motif cumulant approach (Eq. (8)) than the motif moment approach (Eq. (5)); this is the key advantage motif cumulants. The argument was based on the spectral radii $\Psi(\mathbf{W}^0)$ and $\Psi(\mathbf{W}^0\Theta)$, where $\Theta = \mathbf{I} - \mathbf{u}\mathbf{u}^T$ and $\mathbf{u} = (1, \dots, 1)^T / \sqrt{N}$. Using the matrix expression of motif statistics (see Appendix Eq. (18-20)), it is straightforward to see that those spectral radii are related to the asymptotic rate of decay of moments $\mu_{n,m}$ [10] and cumulants $\kappa_{n,m}$ respectively. The faster decay of cumulants vs. moments is therefore reflected by $\Psi(\mathbf{W}^0\Theta)$ being much smaller than $\Psi(\mathbf{W}^0)$. This is indeed the case for networks with sufficiently “homogeneous” connectivity [28], cf. [10]. The goal of this section is to extend arguments of this type to networks with heterogeneous architectures. In doing so, we will reveal why network partitioning can work so well, and describe when it should be applied to a general network.

First, we review the arguments in [28] for statistically homogeneous (i.e., Erdős-Rényi) networks. Here, the spectrum of \mathbf{W}^0 is characterized by a bulk part with many eigenvalues distributed over a region near 0 in the complex plane, and one single positive eigenvalue with much larger magnitude. This latter eigenvalue determines $\Psi(\mathbf{W}^0)$ (from the Perron-Frobenius theorem [41], cf. [42]), and therefore the rate of decay of the moments $\mu_{n,m}$. To study $\Psi(\mathbf{W}^0\Theta)$, and therefore the rate of decay of the motif cumulants, we first define the “PF vector” as the eigenvector associated with the outlying eigenvalue of \mathbf{W}^0 . As a reflection of the underlying homogeneity, the PF vector is close to $\mathbf{e} = (1, \dots, 1)^T$. However, multiplication by Θ essentially removes the eigenvalue associated to this vector from the spectrum of $\mathbf{W}^0\Theta$, since $\mathbf{W}^0\Theta\mathbf{e} = \mathbf{W}^0\mathbf{0} = 0$. This leads to the significant reduction of

$\Psi(\mathbf{W}^0\Theta)$ compared to $\Psi(\mathbf{W}^0)$.

To extend such intuition to networks with heterogeneous architectures, we need to answer two questions: First, what is the PF vector for heterogeneous networks? Second, how does dividing a network into subpopulations change the (effective) Θ , and the resulting spectrum?

We first observe that for many networks, the PF vector is approximately the (in) degree list, denoted as \mathbf{d} (normalized to unit L_2 -norm). In particular, we have found numerically that this is the case for stochastic block models and the Barábasi-Albert networks we consider (see Fig. 10 in Appendix). We will use this observation about the PF vector in making intuitive arguments below, but first pause to make some general, heuristic comments as to its possible justification. We begin by referring back to the case of Erdős-Rényi networks, where the PF vector approximately $\propto \mathbf{e}$ as stated above; and for large matrices, \mathbf{e} will also be approximately proportional to \mathbf{d} with small (relative) error. Now looking at the ensemble average $\mathbf{E}\{\mathbf{W}^0\} \propto \mathbf{e}\mathbf{e}^T$ and observe that \mathbf{e} is the (exact) PF vector for this average matrix $\mathbf{e}\mathbf{e}^T$. Thus the PF vector for the ensemble average and for realizations of the adjacency matrices agree — although this relies on the probabilistic structure of the underlying random matrices in a much more complicated way than we attempt to describe. Next, for a more general graph model, consider an adjacency matrix with an ensemble average that can be written in rank-one form: $\mathbf{E}\{\mathbf{W}^0\} = \mathbf{a}\mathbf{b}^T$ (where \mathbf{a}, \mathbf{b} are column vectors with nonnegative entries). The PF vector for $\mathbf{E}\{\mathbf{W}^0\}$ is \mathbf{a} ; moreover, this is once again proportional to the (average) in-degree list. Drawing a rough analogy with the Erdős-Rényi case suggests a possible reason for why the PF vector for individual adjacency matrices \mathbf{W}^0 are also found to be approximately proportional to \mathbf{d} — although this argument is not rigorous.

We now discuss how to use the fact that the PF vector $\propto \mathbf{d}$ to best partition a network into subpopulations. Recall that the subpopulation theory can be viewed as formally substituting the scalar motif moment and cumulant quantities in the original theory with $b \times b$ matrices (Eq. (29-31)). In [28], we showed that the matrix expression for $\kappa_{n,m}$ and $\mu_{n,m}$ are given by Eqs. (18-20), where repetitive factors such as $\mathbf{W}^0\Theta_B$ appear in places of $\mathbf{W}^0\Theta$. Here Θ_B is a block diagonal generalization of Θ for the subpopulation approach. In particular,

$$\Theta_B = \begin{pmatrix} \Theta_1 & & \\ & \ddots & \\ & & \Theta_b \end{pmatrix}, \quad (9)$$

where each diagonal block corresponds to a subpopulation. Here $\Theta_i = \mathbf{I}_{N_i} - \mathbf{u}_{N_i}\mathbf{u}_{N_i}^T$ (where $\mathbf{u}_{N_i} = (1, \dots, 1)^T / \sqrt{N_i}$) is an “original” Θ matrix, simply defined with population size N_i .

Combining the above observations, we look for a partition of the network that will bring $\mathbf{W}^0\Theta_B\mathbf{d}$ as close to 0 as possible. First, consider the stochastic block model. Note that the Θ_B we defined above will map to $\mathbf{0}$ any vector that is piecewise constant over the indices of each subpopulation. Therefore, if we choose the network partition naturally provided by the stochastic blocks themselves, we obtain $\mathbf{W}^0\Theta_B\mathbf{d} = 0$. As expected, this partitioning results in very rapid decay of motif cumulants, and hence an ability to predict network coherence with only very low order motifs (here, order 1; see Fig. 4(a)).

For the Barábasi-Albert network, there are no “natural” subpopulations, but partitioning

still leads to a significant improvement in predictions of network coherence. In this case, continue to divide the network into just two subpopulations (Fig. 4 (b)). The goal is to perform this division in such a way that will minimize $\|\mathbf{W}^0 \Theta_B \mathbf{d}\|_2$. In practice, we instead consider the simpler question of minimizing $\|\Theta_B \mathbf{d}\|_2$ as an approximation. As noted above, $\|\Theta_B \mathbf{d}\|_2$ measures the error of a piecewise constant (over the indices of subpopulations) approximation of \mathbf{d} . In Fig. 5, we plot this error against a threshold parameter in node degree that is chosen to partition the network; this shows that the error is minimized at a cut-off degree ranking of roughly 30-40 (across different random draws of a Barábasi-Albert network with the same parameters). As expected from our heuristic arguments, this value is close to the value of the threshold that gave the most rapid convergence of the cumulant-based estimates of network covariance (degree ranking = 50, Fig. 5).

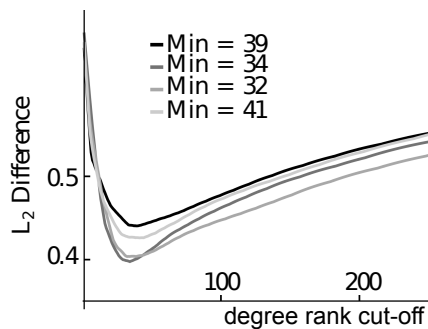


FIG. 5: L_2 norm of the difference between the degree list (normalized) and the piecewise constant vector (see text) given by a certain cut-off ranking of the degrees. Different shades are 4 realizations of Barábasi-Albert networks (with same parameters). The legend is the cut-off degree ranking that achieves the minimum of difference.

Up to this point we have defined motif cumulants, and shown how they can be used to make accurate predictions of the coherence in the activity across a network. All of these results were for second-order correlations (i.e., covariances) averaged across node pairs. We next extend the theory of motif cumulants to predict correlations of arbitrary order.

V Higher order correlations

Here we show how to generalize our theory to relate higher order statistics of a network's dynamics to its architecture. While the second-order results above can be used for both finite-valued stochastic systems (i.e., OU and jump processes) and coupled point processes, the higher-order results are *only valid in their present form for finite-valued stochastic systems* (not point processes with delta function pulses). Extensions to higher-order coherence for interacting point processes are nontrivial and will be tackled elsewhere.

The k^{th} order cross-covariance function for the processes in Eq. (1) are defined using joint

cumulants of random variables,

$$\mathbf{C}_{y[k]}^{i_1 i_2 \dots i_k}(\tau_1, \dots, \tau_{k-1}) := \kappa(y_{i_1}(t), y_{i_2}(t + \tau_1), \dots, y_{i_k}(t + \tau_{k-1})). \quad (10)$$

A generalization of the Wiener-Khinchin theorem relates the Fourier transform of the higher order cumulant to the polyspectra $\mathbf{S}_{y[k]}^{i_1 i_2 \dots i_k}$ [43] defined via the Fourier transform of the processes.

$$\begin{aligned} \mathcal{F}(\mathbf{C}_{y[k]}^{i_1 i_2 \dots i_k}) &= \mathbf{S}_{y[k]}^{i_1 i_2 \dots i_k} = \kappa(\tilde{y}_{i_1}(\omega_1 + \dots + \omega_{k-1}), \tilde{y}_{i_2}(\omega_1), \dots, \tilde{y}_{i_k}(\omega_{k-1})) \\ &:= \lim_{T \rightarrow \infty} \frac{1}{T} \sum_{\chi} (|\chi| - 1)! (-1)^{|\chi|-1} \prod_{B \in \chi} \mathbf{E} \left\{ \prod_{j \in B} \tilde{y}_{i_j}(\omega_{j-1}) \right\} \delta \left(\sum_{j \in B} \omega_j \right) \end{aligned} \quad (11)$$

Here $\omega_0 = -\sum_{j=1}^{k-1} \omega_j$, $\tilde{y}_{i_j}(\omega) = \int_0^T dt e^{-2\pi i \omega t} (y_{i_j}(t) - \mathbf{E}[y_{i_j}(t)])$, $\delta(z) = 1$ when $z = 0$ and $\delta(z) = 0$ otherwise. The first sum is over all partitions χ of set $\{1, \dots, k\}$, and B , as an element of χ , is a subset of $\{1, \dots, k\}$, $|\chi|$ is the number of partitions in χ . To illustrate this formula, we first note that, at third order, it reduces exactly to the ‘‘bispectrum’’ [44, 45, 43]

$$\mathcal{F}(\mathbf{C}_{y[3]}^{i_1 i_2 i_3}(\tau_1, \tau_2)) = \mathbf{S}_{y[3]}^{i_1 i_2 i_3}(\omega_1, \omega_2) := \mathbf{E}[\tilde{y}_{i_1}(\omega_1 + \omega_2) \tilde{y}_{i_2}(\omega_1) \tilde{y}_{i_3}(\omega_2)].$$

It is easy to see that Eq. (11) is multilinear in the variables \tilde{y}_{i_j} . Using Eq. (2), we can therefore generalize Eq. (3) to obtain the polyspectra of the processes \mathbf{y} in terms of that for \mathbf{x} via the propagation matrix $\tilde{\mathbf{P}} = (\mathbf{I} - \tilde{A}\mathbf{W})^{-1}$:

$$\mathbf{S}_{y[k]}^{i_1 i_2 \dots i_k}(\omega_1, \dots, \omega_{k-1}) = \sum_{j_1, \dots, j_k} \tilde{\mathbf{P}}_{i_1 j_1}(\omega_0) \tilde{\mathbf{P}}_{i_2 j_2}(\omega_1) \dots \tilde{\mathbf{P}}_{i_k j_k}(\omega_{k-1}) \mathbf{S}_{x[k]}^{j_1 j_2 \dots j_k}(\omega_1, \dots, \omega_{k-1}). \quad (12)$$

For example, replacing Gaussian white noise which appeared in the OU process with ‘‘Poisson kicks’’, *i.e.* considering a shot noise process, yields non-zero $\mathbf{S}_{x[3]}$.

Next, expanding $\tilde{\mathbf{P}} = \sum_{n=0}^{\infty} (\tilde{A}\mathbf{W})^n$ in Eq. (12) leads to an expression for polyspectra analogous to Eq. (5):

$$\langle \mathbf{S}_{y[k]} \rangle / S_{x[k]} = \frac{1}{N^{k-1}} \sum_{n_1, \dots, n_k=0}^{\infty} g^{|n|} \boldsymbol{\mu}_{n_1, \dots, n_k}, \quad (13)$$

where $|n| = \sum_{i=1}^k n_i$ and $g = N\tilde{A}w$ as defined in Eq. (5). The motif moments $\boldsymbol{\mu}_{n_1, \dots, n_k} = \sum_{i_1, \dots, i_k, j} (\mathbf{W}^{0n_1})_{i_1 j} \dots (\mathbf{W}^{0n_k})_{i_k j} / N^{|n|+1}$. For simplicity, in the formula above we again set $\omega_1 = \dots = \omega_{k-1} = 0$, and assume homogeneous dynamics for each node. Here, $\mathbf{S}_{x[k]}^{i_1 i_2 \dots i_k} = S_{x[k]} \delta^{i_1 i_2 \dots i_k}$ is a diagonal tensor, since the $\{x_i\}$ comprise an uncoupled and uncorrelated network.

The most interesting aspect of Eq. (13) are the motif moments $\boldsymbol{\mu}_{n_1, \dots, n_k}$. For dynamical coherence (and hence polyspectra) of order k , these motif moments are the frequencies of k -branch motifs with n_j nodes on each branch. Fig. 6(a) illustrates such a motif $\boldsymbol{\mu}_{1,1,1}$, for

$k = 3$ branches and $n_j \equiv 1$ node on each branch. Importantly, these k -branch motifs are the only ones that appear at each order in the series of Eq. (13).

We note that higher-order correlations for more general cases, such as variable connection weights, heterogeneity in node dynamics, and common input can be treated similarly, using techniques in [28].

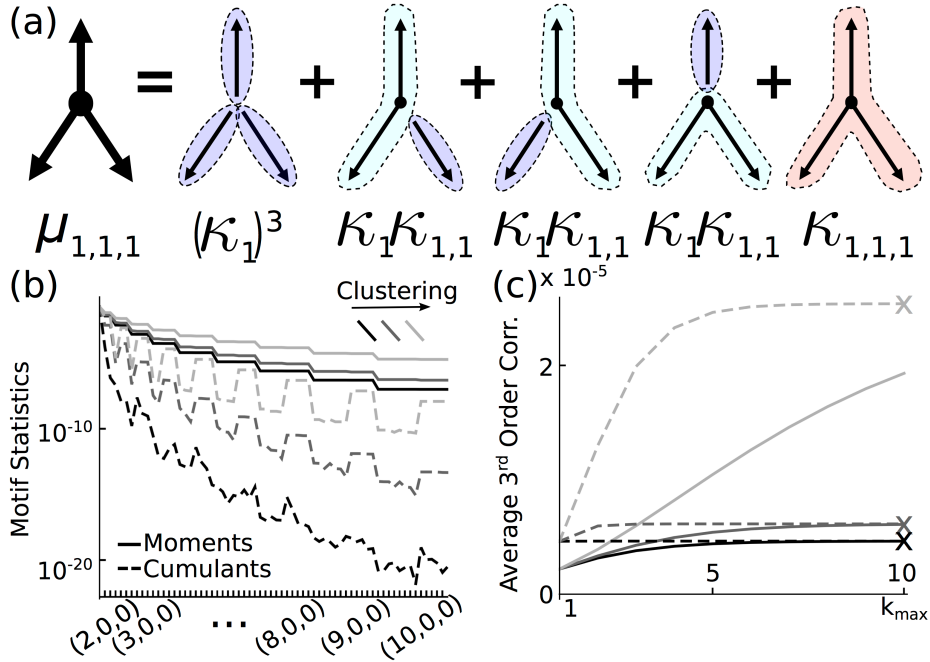


FIG. 6: (a) Cumulant decomposition of a three-branch motif. Panels (b) and (c) are counterparts of Fig. 3(b) and (c) for three-branch motifs and bispectra: (b) decay of motif moments and cumulants with respect to order and (c) convergence estimated third order correlations by two approaches. In (b), the (n, m, l) motifs are again increasingly ordered according to the order $n + m + l$. By symmetry, only motifs with $n \geq m \geq l$ are listed. Within each order, motifs are arranged by lexicographical order of n, m and l , except that motifs with $l \neq 0$ are listed first.

Thus far, we have shown via Eq. (13) how network motifs — quantified by the motif moments μ_{n_1, \dots, n_k} — contribute to higher-order dynamical correlations. The solid lines in Fig. 6(b) show that the motif moments can decay slowly. The consequence is that motifs of high order (up to 10 or beyond) can be required in order to predict third-order correlations via motif moments (Fig. 6(c), solid lines).

This motivates us to develop a prediction of dynamical coherence that will converge with only motifs of smaller size. To do this, we next generalize the motif cumulant approach to higher orders dynamical correlation. First, we define motif cumulants via their relationship with motif moments. Specifically, we relate the motif moments $\{\mu_{*}\}$ and motif cumulants $\{\kappa_{*}\}$ ($*$ stands for multiple indices, see below) via a combinatorial expression. This expression corresponds to the decomposition shown in Fig. 6(a) (cf. Fig. 4(a)), where we have

decomposed a k branch motif into motifs with k and fewer branches.

In more detail, one may enumerate this decomposition explicitly, just as in Eqs. (6,7), according to how a k -branch motif is partitioned at the “root” of the branches (the sum over χ in Eq. (14)) — in other words, by which of the k -branches are grouped together as one component in the decomposition. To see what this means, examine the coloring in Fig. 6(a): for different terms in the decomposition, the components with that are shaded with the seam color have been grouped together. The remaining enumeration is about how each branch breaks up (into chains, the sum over π_i in in Eq. (14)).

$$\boldsymbol{\mu}_{n_1, \dots, n_k} = \sum_{\pi_1, \dots, \pi_k} \left(\prod_{i=1}^k \prod_{j=2}^{t_i} \boldsymbol{\kappa}_{B_j^i} \right) \left(\sum_{\chi} \prod_{\{i_1, \dots, i_s\} \in \chi} \boldsymbol{\kappa}_{B_1^{i_1}, \dots, B_1^{i_s}} \right) \quad (14)$$

Here $\pi_i = \{B_1^i, \dots, B_{t_i}^i\}$ is an ordered partition of n_i , χ is a partition of the set $\{1, \dots, k\}$, and $\{i_1, \dots, i_s\}$ is one subset of indices that are grouped according to the partition χ .

A generalization of Prop. 4.1 in [28], allows us to extend Eq. (8) to predict network-averaged higher order correlations in terms of motif cumulants (proof in Appendix V):

$$\frac{\langle \mathbf{S}_{y[k]} \rangle}{S_{x[k]}} = \frac{1}{N^{k-1}} \left(1 - \sum_{n=1}^{\infty} g^n \boldsymbol{\kappa}_n \right)^{-k} \left(\sum_{\pi} f(\pi) \prod_{B \in \pi, B > 1} \left(\sum_{n_1, \dots, n_B=1}^{\infty} g^{|n|} \boldsymbol{\kappa}_{n_1, \dots, n_B} \right) \right), \quad (15)$$

where π is an partition of integer k . The Faà di Bruno coefficient $f(\pi)$ is the number of partitions of set $\{1, \dots, k\}$ that correspond to a partition π of integer k . An explicit formula for $f(\pi)$ is included in Appendix E. For example, the motif cumulant expansion of the average third order correlation is

$$\frac{\langle \mathbf{S}_{y[3]} \rangle}{S_{x[3]}} = \frac{1}{N^2} \left(1 - \sum_{n=1}^{\infty} g^n \boldsymbol{\kappa}_n \right)^{-3} \left(1 + 3 \sum_{l,m=1}^{\infty} g^{l+m} \boldsymbol{\kappa}_{l,m} + \sum_{l,m,n=1}^{\infty} g^{l+m+n} \boldsymbol{\kappa}_{l,m,n} \right). \quad (16)$$

Fig. 6(b-c) are counterparts of Fig. 3(b-c) that compare motif moment and cumulant approaches for stochastic block networks. They show numerically that our observations for pairwise correlations generalize to higher orders (see also Appendix Fig. 8 when applied to the Barabasi-Albert network). First, we show that higher order correlations can depend significantly on long paths through the network (motif moments, solid lines). Second, when predicting average correlation from only motif statistics up to a given order, an approximation in terms of motif cumulants is more accurate than one in terms of motif moments (panel (c)). Third, the order of motif statistics needed to approximate correlations again increases with network homogeneity (compare lines with different shades).

Finally, the subpopulation approach generalizes to higher order and offers similar advantages in predicting correlations from lower-order motif cumulants (see Appendix G and Fig. 9).

VI Conclusion

Network motifs have been used previously to link local network connectivity and global coherence in networks with linearly interacting components [10, 27, 28]. Here, we developed this theory in order to make it both more general and more applicable in practice. We first showed that a motif-based approach introduced in prior work has a complete probabilistic interpretation in terms of quantities closely related to key concepts in statistics. We refer to these as motif cumulants.

Next, we showed that the link between network architecture and dynamical correlation – through motif cumulants – can be *complex* in networks exhibiting clustering and heterogeneity. This complexity can result in the apparently irreducible contribution of long paths to network-wide coherence. However, with network heterogeneity in mind, the methods of motif cumulants can be extended to reduce this complexity – and hence the size and number of the network features that must be sampled empirically – substantially. Finally, we showed how the theory naturally extends to higher-order dynamical correlations, for a broad subset of the dynamical models under study. This provides a direct link between local network architecture and global dynamics at every order.

An important feature of our approach for experimental settings is that the prevalence of only a limited number of motifs is needed in order to predict network-wide correlation. Moreover, these motifs are small, involving only a few nodes at a time. This property could provide a way forward in experimental settings – as in studies of networks of genes [46] or neurons [2, 3] – in which networks are quantified by sampling a limited number of edges measured simultaneously. The resulting motif prevalences are precisely the quantities needed to define the motif cumulants that are at the core of our approach.

The present results suggest many opportunities for future research. At the top of the list is extending the connection between network motifs and higher-order dynamical correlations to apply to coupled point process models. Somewhat surprisingly, we have found both numerically and analytically (in special cases) that the linear response approach (Eq. (12)) that extends to all orders for finite-valued stochastic processes fails to extend beyond second order for coupled point process models, where each node generates “spike” events (data not shown). Future research will explore modifications of the linear response approach that may re-establish a useful description of higher order correlations for these network models. This would open the door to studies of plasticity and learning of network connections in neural systems, where interactions are governed by point-like spike times [47].

We close by mentioning two further extensions of special interest. The first concerns applications to stimulus-encoding networks. In this setting, there is a heterogeneous network, built of groups of nodes which each have different connectivity rules and, importantly, differently tuned responses to an external stimulus. Networks with spatial structure provide a natural way in which such connectivity and responses might develop. For such a network, our subpopulation motif approach could predict the levels of dynamical correlation within and between each group of nodes. From here, decoding techniques could quantify the level of information that the neural groups carry about the stimulus itself, and how this depends on the correlation structure induced by different network motifs [19, 20, 21, 22, 23, 24, 48, 49].

A final open problem concerns the invertibility of the architecture-to-dynamics question considered here. Given measurements of network-wide coherence, what can we conclude about network architecture? The network motif approach can narrow down the possibilities, especially when higher-order correlations are considered, but we do not yet know what additional assumptions are required to yield a unique solution.

Acknowledgements

We thank C. Hoffman, K. Bassler and B. Doiron for helpful insights and suggestions. This work was supported by NSF grant DMS-1122094, a joint NSF/NIGMS grant R01GM104974, and a Texas NHARP award to KJ, and by a Career Award at the Scientific Interface from the Burroughs Wellcome Fund and NSF Grants DMS-1056125 and DMS-0818153 to ESB.

Appendix

Table I: Notations

N, N_α	size of the whole population or subpopulation α
y_i, \mathbf{y}	activity of node i or that for all nodes combined as a column vector
x_i, \mathbf{x}	baseline activity of node i in the absence of coupling between nodes
$A_i(t)$	linear response kernel of node i
\mathbf{W}, \mathbf{W}^0	connection and adjacency matrix
w	connection strength
$g = N\tilde{A}w$	effective coupling strength
$\mathbf{C}_y(\tau)$	the matrix with cross-covariances of all node pairs of \mathbf{y} [35]
$\mathbf{C}_{y[k]}$	the k -tensor with all k -th order correlations of \mathbf{y} , Eq. (10)
$\mathbf{S}_y(\omega), \mathbf{S}_{y[k]}$	Frequency domain counterparts of $\mathbf{C}_y(\tau)$ and $\mathbf{C}_{y[k]}$, see [36] and Eq. (11)
μ_*, κ_*	motif moment and cumulant, $*$ stands for any subscript describing the length of branches, such as n or n, m , Eq. (5, 6-7,13,14)
$\pi, B \in \pi$	partition (or ordered partition) of an integer and its components
$\chi, \{i_1, \dots, i_s\} \in \chi$	partition of a set S and its components (a subset of S)
$\tilde{\mathbf{P}} = (\mathbf{I} - \tilde{A}\mathbf{W})^{-1}$	propagation factor
$\langle \cdot \rangle$	empirical average of matrix or tensor (sum of entries divided by their number)
$\mathcal{F}(z)$ or \tilde{z}	Fourier transform of z (transform taken entry-wise if z is a matrix or tensor)
\bar{z}	complex conjugate
\mathbf{W}^T	matrix transpose
$\Psi(\mathbf{W})$	spectral radius

A Relating the Ornstein-Uhlenbeck model to Eq. (1) of the main text

We used a simplified form of the canonical Ornstein-Uhlenbeck (OU) model in all examples where we consider second-order statistical quantities. This model is related to Eq. (1) in the main text by writing the dynamics

$$\dot{\mathbf{y}} = -\mathbf{\Lambda}\mathbf{y}(t) + \mathbf{W}\mathbf{y}(t) + \boldsymbol{\xi}(t). \quad (17)$$

where $\mathbf{y}(t) = (y_1(t), \dots, y_N(t))^T$. The diagonal matrix $\mathbf{\Lambda} = \tau^{-1}\mathbf{I}$ sets the intrinsic timescale of the nodes, and the column vector $\boldsymbol{\xi}(t)$ is composed of independent white noise processes. Eq. (17) above is then equivalent to Eq. (1) of the main text with $A_i(t) = A(t) = e^{-t/\tau}\Theta(t)$. Upon coupling, the baseline activity of a node in the network, $\mathbf{x}_i(t) = (A * \boldsymbol{\xi})(t)$, is perturbed by filtered input from other nodes, $A * \sum_j \mathbf{W}_{ij}y_j(t)$.

B Further examples

Here we provide details of several computational findings referred to in the main text. Each addresses the generality and applicability of our results. First, Fig. 7 shows that our main results contrasting motif moments and cumulants hold for the Barábasi-Albert network model, which has significantly more complex structure than the stochastic block models studied in Fig. 3 of the main text.

Next, Figs. 8 and 9 present analogous results for third-order correlations in network output. Specifically, Fig. 8 shows that these third-order correlations depend significantly on the details of the underlying graph structure (i.e., the degree of clustering). Moreover, this dependence can be efficiently predicted via motif cumulants. Fig. 9 demonstrates that the subpopulation approaches continue to enhance the accuracy of our predictions – if the populations are correctly defined, levels of triplet correlations can be predicted from lower-order motifs.

Fig. 10 provide numerical evidence for our claim that the PF vector for a general class of networks is closely approximated by the degree list (see Sec. C).

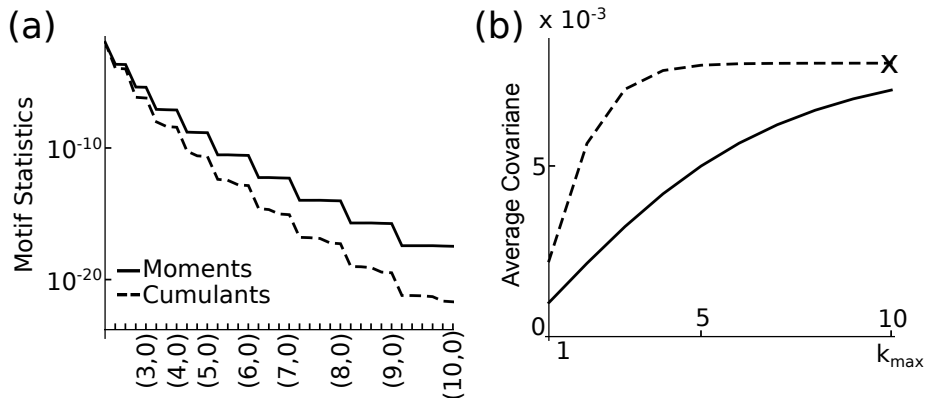


FIG. 7: Same as Fig. 3(b,c) of the main text but for the Barábasi-Albert model. (a) The magnitude of motif cumulants (dashed lines) and moments (solid lines) for a Barábasi-Albert model network. Motifs (n, m) , $n \geq m$ are grouped first by $n + m$ and then arranged by increasing n . (b) Approximations of average covariances using motif moments (truncating Eq. (5), solid lines) and cumulants (truncating Eq. (8), dashed lines) up to order k_{\max} . Exact values (direct evaluation of Eq. (3)) are labeled by crosses: a Barábasi-Albert network of size 1000 and connection probability 0.01.

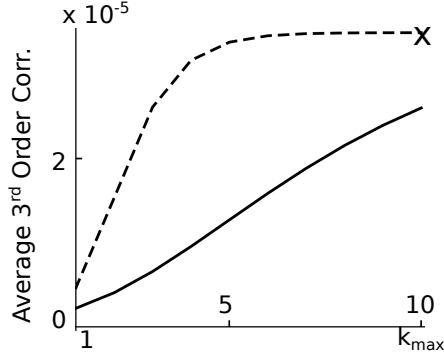


FIG. 8: Same plot as Fig. 7(b) but for average third order correlations $\langle \mathbf{S}_{y[3]} \rangle / S_{x[3]}$. Approximations using motif moments (solid lines) and cumulants (dashed lines) up to order k_{\max} for a Barábasi-Albert network of size 1000 and connection probability 0.01.

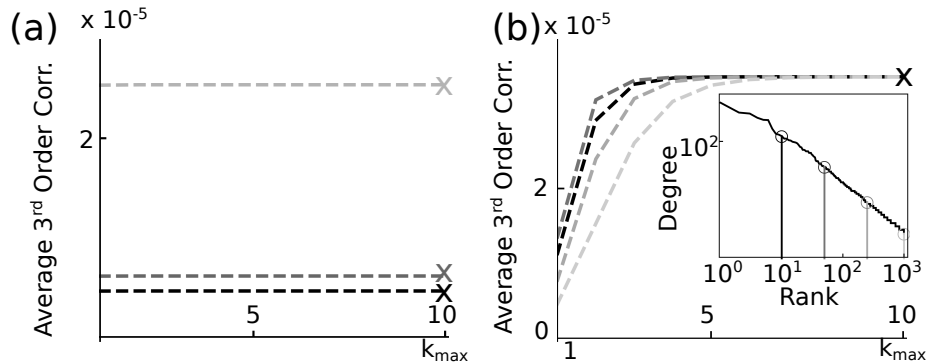


FIG. 9: Same plots as Fig. 4 of the main text but for average third order correlations $\langle \mathbf{S}_{y[3]} \rangle / S_{x[3]}$. Approximations using the subpopulation cumulant approach by truncating at order k_{\max} , the exact values (direct evaluation of Eq. (12) of the main text) are labeled by crosses: (a) stochastic block model networks of Fig. 3 of the main text (the colors are the same) divided into two subpopulations with differing connectivities; (b) the Barábasi-Albert network of SI Fig. 7 divided into two subpopulations according to different thresholds on the sum of in- and out-degrees (different colors, see also the inset, which displays the cutoffs).

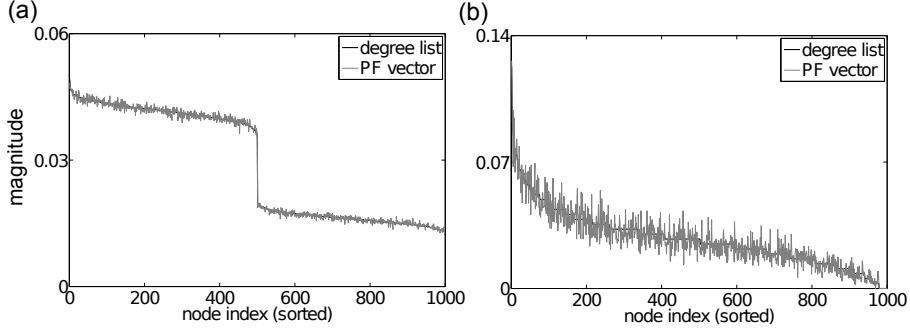


FIG. 10: Comparing the PF vector (gray) and the in-degree list (black) for a stochastic block network (a) and a Barabasi-Albert network (b). The vectors are normalized to have unit L_2 norm and plotted by the indices of nodes, which are ordered in descending in-degree. The stochastic block network has $s_1 = 1.44\sqrt{0.2}$ and is the same one in Fig. 3 (b-c). The Barabasi-Albert network is the same one in Fig. 4 (b).

C Details of numerical results

Here we provide a detailed description of the computational examples provided in the main text and Supplementary Information. This includes all parameters describing the dynamics of nodes and connections, and our methods of generating random networks.

In Fig. 2 of the main text, we calculated correlations for an OU system (see Eq. (17) of the main text) with $\tau = 1$, ξ having unit intensity, and

$$\mathbf{W} = \begin{bmatrix} 0 & -0.75 \\ -0.75 & 0 \end{bmatrix}.$$

In plots of approximations of average second and third order covariances, i.e. Fig. 3(b), 4(a,b) of the main text, SI Figs. 7(b), 8(a,b), and 9(a,b), the parameters \tilde{A} and w are chosen so that $N\tilde{A}wp = 0.4$. Note that the choice of S_x (resp. $S_{x[3]}$ at third order) will not affect the normalized quantity $\langle \mathbf{S}_y \rangle / S_x$ (resp. $\langle \mathbf{S}_{y[3]} \rangle / S_{x[3]}$), and can be set to 1.

The Barabasi-Albert networks in Fig. 4(b), and SI Figs. 7(a,b), 8(b), and 9(b) are generated by a directed Barabasi-Albert model similar to that in [40]. One starts with a “core” of Np nodes, randomly connected with connection probability 0.5. After that, $N - Np$ nodes are added to the graph. When adding a new node $i + 1$, it will form exactly Np connections with the existing nodes $1, \dots, i$. Those connections are distributed among existing nodes according to probabilities that are proportional to the sum of in- and out- degree of each node. The direction of the connection, whether into node $i + 1$ or out of node $i + 1$, is chosen independently with probability 0.5. The code implementing this algorithm is available upon request.

D Explicit expressions for motif cumulants

Here, we will prove that the following matrix expressions for κ_n and $\kappa_{n,m}$ introduced in [28] are equivalent to the recursive definition in Eqs. (6,7) of the main text:

$$\begin{aligned}\kappa_n &= \frac{1}{N^{n+1}} \sum_{i,j} \underbrace{(\mathbf{W}^0 \Theta \mathbf{W}^0 \dots \Theta \mathbf{W}^0)}_{n \text{ factors of } \mathbf{W}^0}{}_{ij} \\ &= \frac{1}{N^n} \mathbf{u}^T [(\mathbf{W} \Theta)^{n-1} \mathbf{W}] \mathbf{u} \\ &= \frac{1}{N^n} \mathbf{u}^T \mathbf{W}_n^\theta \mathbf{u},\end{aligned}\tag{18}$$

$$\begin{aligned}\kappa_{n,m} &= \frac{1}{N^{n+m+1}} \sum_{i,j} \underbrace{(\mathbf{W}^0 \Theta \mathbf{W}^0 \dots \Theta \mathbf{W}^0)}_{n \text{ factors of } \mathbf{W}^0} \Theta \underbrace{\mathbf{W}^{0T} \Theta \mathbf{W}^{0T} \dots \Theta \mathbf{W}^{0T}}_{m \text{ factors of } \mathbf{W}^{0T}}{}_{ij} \\ &= \frac{1}{N^{n+m}} \mathbf{u}^T [(\mathbf{W} \Theta)^{n-1} \mathbf{W} \Theta \mathbf{W}^T (\Theta \mathbf{W}^T)^{m-1}] \mathbf{u} \\ &= \frac{1}{N^{n+m}} \mathbf{u}^T \mathbf{W}_n^\theta \Theta \mathbf{W}_m^\theta \mathbf{u},\end{aligned}\tag{19}$$

where

$$\mathbf{W}_n^\theta = [\mathbf{W}^0 \Theta]^{n-1} \mathbf{W}^0$$

and $\mathbf{u} = (1, \dots, 1)^T / \sqrt{N}$, $\mathbf{H} = \mathbf{u} \mathbf{u}^T$, $\Theta = \mathbf{I} - \mathbf{H}$.

We see that $\mathbf{W}^0 \Theta$, $\Theta \mathbf{W}^T$ are recurring factors in κ_n and $\kappa_{n,m}$. Using the relation of spectral radius and matrix norm [10], one can show that the asymptotic decay speed of κ_* is determined by the spectral radii of these factors. Interestingly, it is easy to show that $\Psi(\mathbf{W}^0 \Theta) = \Psi(\Theta \mathbf{W}^0 \Theta) = \Psi(\Theta \mathbf{W}^0)$ hence these spectral radii coincide. A similar argument relates the decay of μ_* with $\Psi(\mathbf{W}^0)$ (Eq. (20)).

We prove only that Eq. (19) holds, since a nearly identical, but simpler, proof verifies Eq. (18). First, recalling that $\mu_{n,m} = \langle \mathbf{W}^{0n} (\mathbf{W}^{0m})^T \rangle / N^{n+m-1}$, it is straightforward to show that

$$\mu_{n,m} = \frac{1}{N^{n+m}} \mathbf{u}^T (\mathbf{W}^0)^n (\mathbf{W}^{0T})^m \mathbf{u}.\tag{20}$$

Substituting $\mathbf{I} = \Theta + \mathbf{H}$ between every subsequent appearance of the adjacency matrix \mathbf{W}^0 gives

$$\mu_{n,m} = \frac{1}{N^{n+m}} \mathbf{u}^T [\mathbf{W}^0 (\Theta + \mathbf{H})]^{n-1} \mathbf{W}^0 (\Theta + \mathbf{H}) \mathbf{W}^{0T} [(\Theta + \mathbf{H}) \mathbf{W}^{0T}]^{m-1} \mathbf{u}.\tag{21}$$

By expanding across all sums of $\Theta + \mathbf{H}$ except the central one (between the terms \mathbf{W}^0 , \mathbf{W}^{0T}), and noting that there is an obvious bijection between a pair of compositions of the integers n and m , *i.e.*, $\{n_1, \dots, n_t\} \in \mathcal{C}(n)$, $\{m_1, \dots, m_s\} \in \mathcal{C}(m)$, and a term of the form

$$\left[\prod_{i=1}^{t-1} (\mathbf{W}_{n_i}^\theta \mathbf{H}) \right] [\mathbf{W}_{n_t}^\theta (\Theta + \mathbf{H}) \mathbf{W}_{m_s}^\theta] \left[\prod_{j=1}^{s-1} (\mathbf{H} \mathbf{W}_{m_j}^\theta) \right]$$

we may write (using $\mathbf{H} = \mathbf{u}\mathbf{u}^T$)

$$\begin{aligned}
\boldsymbol{\mu}_{n,m} &= \frac{1}{N^{n+m}} \mathbf{u}^T \left\{ \sum_{\substack{\{n_1, \dots, n_t\} \in \mathcal{C}(n) \\ \{m_1, \dots, m_s\} \in \mathcal{C}(m)}}} \left[\prod_{i=1}^{t-1} (\mathbf{W}_{n_i}^\theta \mathbf{H}) \right] [\mathbf{W}_{n_t}^\theta (\boldsymbol{\Theta} + \mathbf{H}) \mathbf{W}_{m_s}^\theta \mathbf{u}] \left[\prod_{j=1}^{s-1} (\mathbf{H} \mathbf{W}_{m_j}^\theta) \right] \right\} \mathbf{u} \\
&= \frac{1}{N^{n+m}} \sum_{\substack{\{n_1, \dots, n_t\} \in \mathcal{C}(n) \\ \{m_1, \dots, m_s\} \in \mathcal{C}(m)}}} \left[\prod_{i=1}^{t-1} (\mathbf{u}^T \mathbf{W}_{n_i}^\theta \mathbf{u}) \right] [\mathbf{u}^T \mathbf{W}_{n_t}^\theta (\boldsymbol{\Theta} + \mathbf{u}\mathbf{u}^T) \mathbf{W}_{m_s}^\theta \mathbf{u}] \left[\prod_{j=1}^{s-1} (\mathbf{u}^T \mathbf{W}_{m_j}^\theta \mathbf{u}) \right] \\
&= \sum_{\substack{\{n_1, \dots, n_t\} \in \mathcal{C}(n) \\ \{m_1, \dots, m_s\} \in \mathcal{C}(m)}}} \left[\prod_{i=1}^{t-1} \left(\frac{1}{N^{n_i}} \mathbf{u}^T \mathbf{W}_{n_i}^\theta \mathbf{u} \right) \right] \left[\frac{1}{N^{n_t+m_s}} \mathbf{u}^T \mathbf{W}_{n_t}^\theta (\boldsymbol{\Theta} + \mathbf{u}\mathbf{u}^T) \mathbf{W}_{m_s}^\theta \mathbf{u} \right] \\
&\quad \cdot \left[\prod_{j=1}^{s-1} \left(\frac{1}{N^{m_j}} \mathbf{u}^T \mathbf{W}_{m_j}^\theta \mathbf{u} \right) \right]
\end{aligned} \tag{22}$$

If $t = 1$, we define the product $\left[\prod_{i=1}^{t-1} (\mathbf{W}_{n_i}^\theta \mathbf{H}) \right] = \mathbf{I}$.

We now prove Eq. (19) by induction, assuming Eq. (18) holds. First, when $n = m = 1$, the only compositions are trivial (i.e., $\pi_1 = \pi_2 = \{1\}$). Equating in this case the right-hand sides of Eq. (7) of the main text and Eq. (22) gives that

$$\boldsymbol{\kappa}_{1,1} + (\boldsymbol{\kappa}_1)^2 = \frac{1}{N^2} \mathbf{u}^T \mathbf{W}_1^\theta \boldsymbol{\Theta} \mathbf{W}_1^\theta \mathbf{u} + \left(\frac{1}{N} \mathbf{u}^T \mathbf{W}_1^\theta \mathbf{u} \right)^2.$$

Since Eq. (18) for $n = 1$ gives that

$$\boldsymbol{\kappa}_1 = \frac{1}{N} \mathbf{u}^T \mathbf{W}_1^\theta \mathbf{u},$$

we have that Eq. (19) holds for $n = m = 1$. Next, assume Eq. (19) is true for all (p, q) such that $p \leq n$ and $q < m$ or $p < n$ and $q \leq m$. That is, in these cases,

$$\boldsymbol{\kappa}_p = \frac{1}{N^p} \mathbf{u}^T \mathbf{W}_p^\theta \mathbf{u} \text{ (by Eq. (18))} \quad \text{and} \quad \boldsymbol{\kappa}_{p,q} = \frac{1}{N^{p+q}} \mathbf{u}^T \mathbf{W}_p^\theta \boldsymbol{\Theta} \mathbf{W}_q^\theta \mathbf{u}.$$

Making the corresponding substitutions in Eq. (22), the only term we have not accounted for in matching the right-hand side of Eq. (22) to that of Eq. (7) of the main text are the terms corresponding to the pair of compositions $\{n\}, \{m\}$. In Eq. (7) of the main text, the corresponding terms are

$$\boldsymbol{\kappa}_{n,m} + \boldsymbol{\kappa}_n \boldsymbol{\kappa}_m \tag{23}$$

while in Eq. (22), the terms take the form

$$\begin{aligned}
\frac{1}{N^{n+m}} \mathbf{u}^T \mathbf{W}_n^\theta (\boldsymbol{\Theta} + \mathbf{u}\mathbf{u}^T) \mathbf{W}_m^\theta \mathbf{u} &= \frac{1}{N^{n+m}} \mathbf{u}^T \mathbf{W}_n^\theta \boldsymbol{\Theta} \mathbf{W}_m^\theta \mathbf{u} + \left(\frac{1}{N^n} \mathbf{u}^T \mathbf{W}_n^\theta \mathbf{u} \right) \left(\frac{1}{N^m} \mathbf{u}^T \mathbf{W}_m^\theta \mathbf{u} \right) \\
&= \frac{1}{N^{n+m}} \mathbf{u}^T \mathbf{W}_n^\theta \boldsymbol{\Theta} \mathbf{W}_m^\theta \mathbf{u} + \boldsymbol{\kappa}_n \boldsymbol{\kappa}_m,
\end{aligned} \tag{24}$$

where the second equality follows from the inductive assumption. Comparing Eqs. (23,24) gives that

$$\boldsymbol{\kappa}_{n,m} = \frac{1}{N^{n+m}} \mathbf{u}^T \mathbf{W}_n^\theta \boldsymbol{\Theta} \mathbf{W}_m^\theta \mathbf{u},$$

which is exactly Eq. (19), completing the inductive proof.

E Expression of $f(\pi)$

Let ν be the set of unique B 's in π , and for every $B \in \nu$, $\#B$ is the number of repetitions of B in π .

$$f(\pi) = \left(\sum_{B \in \pi} B \right)! \cdot \left(\prod_{B \in \pi} B! \right)^{-1} \cdot \left(\prod_{B \in \pi} \#B! \right)^{-1}. \quad (25)$$

F Proof of Eq. (15)

In order to prove Eq. (15), we will first establish the following result.

Theorem VI.1. *For a pair of motif moments and cumulants $\{\boldsymbol{\mu}_*\}$ and $\{\boldsymbol{\kappa}_*\}$ with up to k branches,*

$$\sum_{n_1, \dots, n_k=0}^{\infty} \boldsymbol{\mu}_{n_1, \dots, n_k} = \left(1 - \sum_{n=1}^{\infty} \boldsymbol{\kappa}_n \right)^{-k} \left(\sum_{\pi} f(\pi) \prod_{B \in \pi, B > 1} \left(\sum_{n_1, \dots, n_B=1}^{\infty} \boldsymbol{\kappa}_{n_1, \dots, n_B} \right) \right), \quad (26)$$

assuming all series converge absolutely and $|\sum_{n=1}^{\infty} \boldsymbol{\kappa}_n| < 1$. The sum with index π is through all partitions of k . When indices for the product are empty, we take the corresponding terms to be 1.

To prove Eq. (15), first note that note that Eq. (14) is ‘‘homogeneous in degree,’’ so that if it is satisfied by with pairs of motif moments and cumulants $\{\boldsymbol{\mu}_*\}$, $\{\boldsymbol{\kappa}_*\}$, it will also be satisfied for scaled pairs $\{g^{|\cdot|} \boldsymbol{\mu}_*\}$, $\{g^{|\cdot|} \boldsymbol{\kappa}_*\}$. Thus, the same relationship holds for scaled motif statistics. Then, apply Theorem VI.1 to Eq. 13, using scaled motif statistics, to obtain the desired Eq. (15).

Proof of Theorem VI.1. First, we rewrite the LHS of Eq. (26), to explicitly account for cases with different n_j nonzero. Specifically, we sum over all possible sets of $k \leq k'$ indices $\{j_1, \dots, j_k\}$ corresponding to the nonzero values of n_j :

$$\sum_{n_1, \dots, n_{k'}=0}^{\infty} \boldsymbol{\mu}_{n_1, \dots, n_{k'}} = \sum_{\substack{\{j_1, \dots, j_k\} \\ \subset \{1, \dots, k'\}}} \sum_{n_{j_1}, \dots, n_{j_k}=1}^{\infty} \boldsymbol{\mu}_{n_{j_1}, \dots, n_{j_k}} \quad (27)$$

We now focus on a fixed k , and without loss of generality, let $\{j_1, \dots, j_k\} = \{1, \dots, k\}$. Applying Eq. (14), we have

$$\begin{aligned} \sum_{n_1, \dots, n_k=1}^{\infty} \boldsymbol{\mu}_{n_1, \dots, n_k} &= \sum_{n_1, \dots, n_k=1}^{\infty} \sum_{\pi_1, \dots, \pi_k} \left(\prod_{i=1}^k \prod_{j=2}^{t_i} \boldsymbol{\kappa}_{B_j^i} \right) \left(\sum_{\chi} \prod_{\{i_1, \dots, i_s\} \in \chi} \boldsymbol{\kappa}_{B_1^{i_1}, \dots, B_1^{i_s}} \right) \\ &= \sum_{\chi} \sum_{B_1^{i_1}, \dots, B_1^{i_s} \geq 1} \prod_{\{i_1, \dots, i_s\} \in \chi} \boldsymbol{\kappa}_{B_1^{i_1}, \dots, B_1^{i_s}} \left(\sum_{n_1, \dots, n_k} \sum_{\pi_1, \dots, \pi_k} \left(\prod_{i=1}^k \prod_{j=2}^{t_i} \boldsymbol{\kappa}_{B_j^i} \right) \right). \end{aligned}$$

In the last equality, we switched the order of summations by pulling the sum over χ to the front. Consequently, for each fixed $\{B_1^{i_1}, \dots, B_1^{i_s}\}$ taken in an outer sum, the $\{\pi_i\}$ and $\{n_i\}$ are restricted to terms that are possible for that $\{B_1^{i_1}, \dots, B_1^{i_s}\}$. Notice that these sums can be factorized as

$$\sum_{n_1, \dots, n_k} \sum_{\pi_1, \dots, \pi_k} \left(\prod_{i=1}^k \prod_{j=2}^{t_i} \boldsymbol{\kappa}_{B_j^i} \right) = \prod_{i=1}^k \left(\sum_{n_i \geq B_1^i} \sum_{\pi_i \ni B_1^i} \prod_{j=2}^{t_i} \boldsymbol{\kappa}_{B_j^i} \right). \quad (28)$$

We next will simplify the factors on the RHS of Eq. (28). First, we shift the (dummy) indices of summation and multiplication to explicitly begin counting at the second block in the branch:

$$\sum_{n_i \geq B_1^i} \sum_{\pi_i \ni B_1^i} \prod_{j=2}^{t_i} \boldsymbol{\kappa}_{B_j^i} = \sum_{n'_i=0}^{\infty} \sum_{\pi'_i} \prod_{j=1}^{t'_i} \boldsymbol{\kappa}_{B_{j+1}^i},$$

where $n'_i = n_i - B_1^i$, $\pi'_i = \pi_i \setminus \{B_1^i\}$ and $t'_i = t_i - 1$ as we exclude the B_1^i component. For simplicity, we will drop the primes in the summation indices, and then let B_j^i range over the components of the resulting partition (thus rewriting $j+1 \rightarrow j$ below). Doing this, and further rearranging the terms, we have

$$\begin{aligned} \sum_{n_i=0}^{\infty} \sum_{\pi_i} \prod_{j=1}^{t_i} \boldsymbol{\kappa}_{B_j^i} &= \sum_{t_i=0}^{\infty} \sum_{n_i \geq t_i} \sum_{\pi_i} \prod_{j=1}^{t_i} \boldsymbol{\kappa}_{B_j^i} \\ &= \sum_{t_i=0}^{\infty} \prod_{j=1}^{t_i} \sum_{B_j^i=1}^{\infty} \boldsymbol{\kappa}_{B_j^i} = \sum_{t_i=0}^{\infty} \left(\sum_{n_i=1}^{\infty} \boldsymbol{\kappa}_{n_i} \right)^{t_i} = \left(1 - \sum_{n=1}^{\infty} \boldsymbol{\kappa}_n \right)^{-1}, \end{aligned}$$

where we have summed the geometric series in the last inequality (note the convergence criterion in the Theorem statement).

Therefore, Eq. (28) and the expression above it yield

$$\begin{aligned}
\sum_{n_1, \dots, n_k=1}^{\infty} \mu_{n_1, \dots, n_k} &= \sum_{\chi} \sum_{B_1^{i_1}, \dots, B_1^{i_s} \geq 1}^{\infty} \prod_{\{i_1, \dots, i_s\} \in \chi} \kappa_{B_1^{i_1}, \dots, B_1^{i_s}} \left(1 - \sum_{n=1}^{\infty} \kappa_n \right)^{-k} \\
&= \left(1 - \sum_{n=1}^{\infty} \kappa_n \right)^{-k} \sum_{\chi} \prod_{\{i_1, \dots, i_s\} \in \chi} \left(\sum_{B_1^{i_1}, \dots, B_1^{i_s} \geq 1}^{\infty} \kappa_{B_1^{i_1}, \dots, B_1^{i_s}} \right) \\
&= (1-q)^{-k} \sum_{\chi} \prod_{\{i_1, \dots, i_s\} \in \chi} \left(\sum_{B_1^{i_1}, \dots, B_1^{i_s} \geq 1}^{\infty} \kappa_{B_1^{i_1}, \dots, B_1^{i_s}} \right),
\end{aligned}$$

where we let $q = \sum_{n=1}^{\infty} \kappa_n$. The above gives a useful expression for the sum over all motifs with exactly k branches of nonzero length. To establish the theorem, we use this expression for different subsets of $\{1, \dots, k'\}$ (hence different k) that occur in Eq. (27). Doing this, we have

$$\sum_{n_1, \dots, n_{k'}=0}^{\infty} \mu_{n_1, \dots, n_{k'}} = \sum_{\substack{\{j_1, \dots, j_k\} \\ \subset \{1, \dots, k'\}}} \sum_{\chi_k} (1-q)^{-k} \prod_{\{i_1, \dots, i_s\} \in \chi_k} \left(\sum_{B_1^{i_1}, \dots, B_1^{i_s} \geq 1}^{\infty} \kappa_{B_1^{i_1}, \dots, B_1^{i_s}} \right)$$

where χ_k is a partition of the set $\{j_1, \dots, j_k\}$ (through we only use the subscript k , χ_k should actually depend on the set $\{j_1, \dots, j_k\}$). We next rearrange this expression. First, we define a lift of each partition χ_k to a partition χ of the set $\{1, \dots, k'\}$, by adding any indices not present in χ_k as individual groups $\{i_{k+1}\}, \dots, \{i_{k'}\}$. Next we split the sum across $\{j_1, \dots, j_k\}$ and χ_k according to their resulting lift χ . This creates an outer sum; here, the range of χ is all possible partitions of $\{1, \dots, k'\}$. Thus, the expression above

$$= \sum_{\chi} \sum_{\chi_k | \chi} (1-q)^{-k} \prod_{\{i_1, \dots, i_s\} \in \chi_k} \left(\sum_{B_1^{i_1}, \dots, B_1^{i_s} \geq 1}^{\infty} \kappa_{B_1^{i_1}, \dots, B_1^{i_s}} \right)$$

The inner sum is over all χ_k , $0 \leq k \leq k'$ whose lift is χ . We can pull out all factors associated with groups in χ_k that has only 1 element. Note each of such group $\{i_r\}$ corresponds to a factor $\sum_{B_1^{i_r} \geq 1}^{\infty} \kappa_{B_1^{i_r}} = q$. Therefore the rest factors in $\prod_{\{i_1, \dots, i_s\} \in \chi_k}$ are $(k - m_2)$ q -factors, where m_2 is the number of indices that are partitioned into a group with more than 1 elements in χ_k (or χ). Thus, the expression above

$$\begin{aligned}
&= \sum_{\chi} \sum_{\chi_k | \chi} (1-q)^{-k} q^{k-m_2} \prod_{\substack{\{i_1, \dots, i_s\} \in \chi_k, \\ s > 1}} \left(\sum_{B_1^{i_1}, \dots, B_1^{i_s} \geq 1}^{\infty} \kappa_{B_1^{i_1}, \dots, B_1^{i_s}} \right) \\
&= (1-q)^{-k'} \sum_{\chi} \prod_{\substack{\{i_1, \dots, i_s\} \in \chi, \\ s > 1}} \left(\sum_{B_1^{i_1}, \dots, B_1^{i_s} \geq 1}^{\infty} \kappa_{B_1^{i_1}, \dots, B_1^{i_s}} \right) \cdot \left(\sum_{\chi_k | \chi} q^{k-m_2} (1-q)^{k'-k} \right).
\end{aligned}$$

For a fixed k , it is easy to see the number of χ_k whose lift being χ is $\binom{k'-m_2}{k-m_2}$. Hence

$$\sum_{\chi_k|\chi} q^{k-m_2}(1-q)^{k'-k} = \sum_{k=0}^{k'} \binom{k'-m_2}{k-m_2} q^{k-m_2}(1-q)^{k'-k} = 1,$$

Finally, the expression above

$$\begin{aligned} &= (1-q)^{-k'} \sum_{\chi} \prod_{\substack{\{i_1, \dots, i_s\} \in \chi, \\ s > 1}} \left(\sum_{B_1^{i_1}, \dots, B_1^{i_s} \geq 1}^{\infty} \boldsymbol{\kappa}_{B_1^{i_1}, \dots, B_1^{i_s}} \right) \\ &= (1-q)^{-k'} \sum_{\pi} f(\pi) \prod_{B \in \pi, B > 1} \left(\sum_{n_1, \dots, n_B=1}^{\infty} \boldsymbol{\kappa}_{n_1, \dots, n_B} \right). \end{aligned}$$

In the last line, since the factor with $\boldsymbol{\kappa}_*$ is the same as long as s is the same, regardless of actual value of i_1, \dots, i_s , we switched from summing over set partitions χ to corresponding integer partitions π of k' . This introduces the $f(\pi)$ factor and finishes the proof (see Eq. (26)). \square

G Subpopulation cumulant approach

The recursive decomposition relationships for subpopulation motif moments and cumulants (all being $b \times b$ matrices) are

$$\boldsymbol{\mu}_n = \sum_{\{n_1, \dots, n_t\} \in \mathcal{C}(n)} \left[\left(\prod_{i=2}^t \boldsymbol{\kappa}_{n_i} \mathbf{E} \right) \boldsymbol{\kappa}_{n_1} \right] \quad (29)$$

$$\boldsymbol{\mu}_{n,m} = \sum_{\substack{\{n_1, \dots, n_t\} \in \mathcal{C}(n) \\ \{m_1, \dots, m_s\} \in \mathcal{C}(m)}} \left(\prod_{i=2}^t \boldsymbol{\kappa}_{n_i} \mathbf{E} \right) (\boldsymbol{\kappa}_{n_1, m_1} + \boldsymbol{\kappa}_{n_1} \mathbf{E} \boldsymbol{\kappa}_{m_1}) \left(\prod_{j=2}^s \mathbf{E} \boldsymbol{\kappa}_{m_j} \right). \quad (30)$$

Here $\mathbf{E} = \text{diag}\{N_1/N, \dots, N_b/N\}$ (b is the number of subpopulations, having sizes N_i , where $\sum N_i = N$) is inserted between each motif cumulant matrix multiplication and yields the appropriate weighted sums for the interpretation of the terms $\boldsymbol{\mu}_{n,m}$ and $\boldsymbol{\kappa}_{n,m}$ as *probabilities*. Specifically, scaling by \mathbf{E} is multiplication by the probability of selecting nodes from respective populations at “breaks” in the motifs.

Let $\langle \mathbf{S}_y \rangle_B$ represent a block-wise average over entries corresponding to each subpopulation. The generalization of Eq. (8) for multi population motif cumulants is [28]:

$$\begin{aligned} \langle \mathbf{S}_y \rangle_B / S_x &:= \mathbf{D} \mathbf{U}^T \mathbf{S}_y \mathbf{U} \mathbf{D} / S_x \\ &= \frac{1}{N} \left(\mathbf{I} - \sum_{n=1}^{\infty} g^n \boldsymbol{\kappa}_n \mathbf{E} \right)^{-1} \left(\mathbf{E}^{-1} + \sum_{n,m=1}^{\infty} g^{n+m} \boldsymbol{\kappa}_{n,m} \right) \left(\mathbf{I} - \sum_{m=1}^{\infty} g^m \mathbf{E} \boldsymbol{\kappa}_m \right)^{-1}. \end{aligned} \quad (31)$$

where $\mathbf{D} = \text{diag}\{1/\sqrt{N_1}, \dots, 1/\sqrt{N_b}\}$, \mathbf{U} is $N \times k$ matrix given by $\mathbf{U} = [\mathbf{u}_1 | \dots | \mathbf{u}_k]$, and $\mathbf{u}_i = (0, \dots, 0, 1, \dots, 1, 0, \dots, 0)^T / \sqrt{N_i}$ is the vector where the nonzero entries appear only at indices that match one of the nodes in the given subpopulation, normalized to unit L_2 norm.

Beyond the similarity in appearance between the single population and multipopulation formulas Eq. (8) and (31), these two can be precisely connected. Define a new product between two matrices (or tensors) as

$$(\mathbf{A} \odot \mathbf{B})_{ij} = \sum_k \mathbf{A}_{ik} \mathbf{B}_{jk} \frac{N_k}{N}. \quad (32)$$

It's easy to see that Eq. (29) and (30) are equivalent to Eq. (6) and (7) when the product is interpreted as \odot . Very much like the ordinary matrix multiplication, \odot is noncommutative, but associative and distributive, which are all that we need for the theory. This shows that Eq. (31) can be proved by identically as the single population case Eq. (8) while interpreting products via \odot .

Such an idea is exactly how we will develop the multipopulation theory for higher order correlations. Under the interpretation of \odot , the relationship among multipopulation motif moments and cumulants can be written as

$$\boldsymbol{\mu}_{n_1, \dots, n_k} = \sum_{\pi_1, \dots, \pi_k} \left(\bigotimes_{i=1}^k \prod_{j=2}^{t_i} \boldsymbol{\kappa}_{B_j^i} \right) \cdot \left(\sum_{\chi \{i_1, \dots, i_s\} \in \chi} \bigodot \boldsymbol{\kappa}_{B_1^{i_1}, \dots, B_1^{i_s}, \cdot} \right) \quad (33)$$

As before $\pi_i = \{B_1^i, \dots, B_{t_i}^i\}$ is an ordered partition of n_i . Moreover, χ is a partition of the set $\{1, \dots, k\}$ and $\{i_1, \dots, i_s\}$ is one set of indices that are grouped together under χ . Here $\boldsymbol{\mu}_{n_1, \dots, n_k}$ (for $k \geq 2$) is a k dimensional tensor: each entry $\mu_{n_1, \dots, n_k}^{\alpha_1, \dots, \alpha_k}$ represents the frequency of a k brach motif with endpoints in subpopulation $\alpha_1, \dots, \alpha_k$ respectively. Notably, there is a third type of quantity appearing in Eq. (33): $\boldsymbol{\kappa}_{B_1^{i_1}, \dots, B_1^{i_s}, \cdot}$, which is a $s+1$ tensor ($s \geq 2$). The extra dimension (represented by the dot in subscript) comes from specifying the subpopulation of the root node, beside the subpopulation of the endpoints. This is the same situation as for one-branch or chain motifs $\boldsymbol{\mu}_{n_1}$ and $\boldsymbol{\kappa}_{B_j^i}$, which are 2-tensors ($b \times b$ matrices) and should formally be written as $\boldsymbol{\mu}_{n_1, \cdot}$ and $\boldsymbol{\kappa}_{B_j^i, \cdot}$; we omit the dot for these chains as long as it is clear from the context. The big \odot product forms an k tensor out of $|\chi|$ factors, in a way similar to a multivariate trace:

$$\left(\bigodot_{\{i_1, \dots, i_s\} \in \chi} \boldsymbol{\kappa}_{B_1^{i_1}, \dots, B_1^{i_s}, \cdot} \right)^{\alpha_1, \dots, \alpha_k} = \sum_{\beta=1}^b \frac{N_\beta}{N} \prod_{\{i_1, \dots, i_s\} \in \chi} \boldsymbol{\kappa}_{B_1^{i_1}, \dots, B_1^{i_s}, \cdot}^{\alpha_{i_1}, \dots, \alpha_{i_s}, \beta}. \quad (34)$$

As an example, if χ only contains one partition, that consisting of the set itself, we define $\boldsymbol{\kappa}_{B_1^1, \dots, B_1^k} := \bigodot \boldsymbol{\kappa}_{B_1^1, \dots, B_1^k, \cdot}$. It's not hard to see that the meaning of the resulting s -tensor $\boldsymbol{\kappa}_{B_1^1, \dots, B_1^k}$ is the motif cumulant with specified subpopulations for the endpoints.

The tensor product “ $\bigotimes_{j=1}^k$ ” in Eq. (33) is simply a weighted version of the ordinary tensor product, that is

$$\left(\bigotimes_{j=1}^k \mathbf{P}_j \cdot \mathbf{A} \right)^{\alpha_1, \dots, \alpha_k} = \sum_{\beta_1, \dots, \beta_k} \left(\prod_{j=1}^k \frac{N_j}{N} (\mathbf{P}_j)_{\alpha_j, \beta_j} \right) \mathbf{A}^{\beta_1, \dots, \beta_k}. \quad (35)$$

Despite the difference in notation between Eq. (33) and (14), the operations share some basic algebraic properties, namely being associative and distributive — which are all that is needed in the proof of Eq. (15). This allows us to derive, with identical arguments, the subpopulation result:

$$\frac{\langle \mathbf{S}_{y[k]} \rangle_B}{S_{x[k]}} = \frac{1}{N^{k-1}} \bigotimes_{i=1}^k \left(\mathbf{I} - \sum_{n=1}^{\infty} g^n \boldsymbol{\kappa}_n \right)^{-1} \cdot \left(\sum_{\chi} \bigodot_{\{i_1\} \in \chi} \mathbf{E}^{-1} \bigodot_{\{i_1, \dots, i_s\} \in \chi, s > 1} \left(\sum_{n_1, \dots, n_s=1}^{\infty} g^{|\mathbf{n}|} \boldsymbol{\kappa}_{n_1, \dots, n_s} \right) \right). \quad (36)$$

Here, the two “ \bigodot ” terms are actually two parts of one single product associated with χ , as defined in Eq. (34). Specifically:

$$\begin{aligned} & \left(\bigodot_{\{i_1\} \in \chi} \mathbf{E}^{-1} \bigodot_{\{i_1, \dots, i_s\} \in \chi, s > 1} \left(\sum_{n_1, \dots, n_s=1}^{\infty} g^{|\mathbf{n}|} \boldsymbol{\kappa}_{n_1, \dots, n_s} \right) \right)^{\alpha_1, \dots, \alpha_k} \\ &= \sum_{\beta=1}^b \frac{N_\beta}{N} \prod_{\{i_1\} \in \chi} (\mathbf{E}^{-1})_{\alpha_{i_1} \beta} \prod_{\{i_1, \dots, i_s\} \in \chi} \boldsymbol{\kappa}_{B_1^{i_1}, \dots, B_1^{i_s}}^{\alpha_{i_1}, \dots, \alpha_{i_s}, \beta}. \end{aligned}$$

We emphasize again that all multiplicative operations in the formula above should be interpreted as for \odot .

However, it is also easy to rewrite this expression using only ordinary products, by inserting the diagonal scaling matrix \mathbf{E} . For example, enumerating the terms for third order correlation ($k = 3$) yields

$$\begin{aligned} \langle \mathbf{S}_{y[3]} \rangle_B / S_{x[3]} &= \frac{1}{N^2} \left(\mathbf{I} - \sum_{l=1}^{\infty} g^l \boldsymbol{\kappa}_l \mathbf{E} \right)^{-1} \otimes \left(\mathbf{I} - \sum_{m=1}^{\infty} g^m \boldsymbol{\kappa}_m \mathbf{E} \right)^{-1} \otimes \left(\mathbf{I} - \sum_{n=1}^{\infty} g^n \boldsymbol{\kappa}_n \mathbf{E} \right)^{-1} \\ &\cdot \left(\mathbf{E}_{[3]}^{-2} + \sum_{l,m=1}^{\infty} g^{l+m} (\boldsymbol{\kappa}_{l,m,\cdot} + \boldsymbol{\kappa}_{l,\cdot,m} + \boldsymbol{\kappa}_{\cdot,l,m}) + \sum_{l,m,n=1}^{\infty} g^{l+m+n} \boldsymbol{\kappa}_{l,m,n} \right). \end{aligned} \quad (37)$$

Here $\mathbf{E}_{[3]}^{-2}$ is a diagonal 3-tensor, with $(\mathbf{E}_{[3]}^{-2})^{\alpha\beta\gamma} = \delta_{\alpha\beta\gamma} \left(\frac{N_\alpha}{N} \right)^{-2}$. $\boldsymbol{\kappa}_{l,\cdot,m}$ and $\boldsymbol{\kappa}_{\cdot,l,m}$ are transpositions of the tensor $\boldsymbol{\kappa}_{l,m,\cdot}$, i.e. $(\boldsymbol{\kappa}_{l,m,\cdot})^{i_1, i_2, i_3} = (\boldsymbol{\kappa}_{l,\cdot,m})^{i_1, i_3, i_2} = (\boldsymbol{\kappa}_{\cdot,l,m})^{i_3, i_1, i_2}$.

References

- [1] P. Bonifazi et al., *The Neuroscientist Comments*, Science (New York, NY) **326**, 1419 (2009).
- [2] S. Song, P. J. Sjöström, M. Reigl, S. Nelson, and D. B. Chklovskii, *Highly nonrandom features of synaptic connectivity in local cortical circuits*, PLoS. Biol. **3**, e68 (2005).
- [3] R. Perin, T. K. Berger, and H. Markram, *A synaptic organizing principle for cortical neuronal groups*, Proc. Natl. Acad. Sci. USA **108**, 5419 (2011).
- [4] R. Milo et al., *Superfamilies of evolved and designed networks.*, Science (New York, NY) **303**, 1538 (2004).
- [5] P. Larimer and B. W. Strowbridge, *Nonrandom local circuits in the dentate gyrus*, J. Neurosci. **28**, 12212 (2008).
- [6] L. Pecora and T. Carroll, *Master Stability Functions for Synchronized Coupled Cell Systems*, Phys. Rev. Lett. **80**, 2109 (1998).
- [7] S. Strogatz, *From Kuramoto to Crawford: Exploring the onset of synchronization in populations of coupled oscillators*, Physica. D. **143**, 1 (2000).
- [8] J. Rinzel and G. B. Ermentrout, *Analysis of neural excitability and oscillations*, in *Methods in neuronal modeling.*, edited by C. Koch and I. Segev, pages 135–169, MIT Press, 1989.
- [9] A. Renart et al., *The asynchronous state in cortical circuits*, Science **327**, 587 (2010).
- [10] V. Pernice, B. Staude, S. Cardanobile, and S. Rotter, *How Structure Determines Correlations in Neuronal Networks*, PLoS. Comput. Biol. **7**, e1002059 (2011).
- [11] V. Pernice, B. Staude, S. Cardanobile, and S. Rotter, *Recurrent interactions in spiking networks with arbitrary topology*, Phys. Rev. E. **85** (2012).
- [12] B. Lindner, B. Doiron, and A. Longtin, *Theory of oscillatory firing induced by spatially correlated noise and delayed inhibitory feedback*, Phys. Rev. E. **72**, 1 (2005).
- [13] E. Schneidman, S. Still, M. J. Berry, and W. Bialek, *Network Information and Connected Correlations*, Phys.Rev. Lett. **91**, 238701 (2003).
- [14] P. Fries, *A mechanism for cognitive dynamics: neuronal communication through neuronal coherence*, Trends Cogn Sci **9**, 474 (2005).
- [15] W. Singer and C. M. Gray, *Visual Feature Integration and the Temporal Correlation Hypothesis*, Annual Review of Neuroscience **18**, 555 (1995).

- [16] E. Salinas and T. J. Sejnowski, *Impact of Correlated Synaptic Input on Output Firing Rate and Variability in Simple Neuronal Models*, J. Neurosci. **20**, 6193 (2000).
- [17] M. Diesmann, M.-O. Gewaltig, and A. Aertsen, *Stable propagation of synchronous spiking in cortical neural networks*, Nature **402**, 529 (1999).
- [18] A. Pikovsky, M. Rosenblum, and J. Kurths, *Synchronization: A Universal Concept in Nonlinear Sciences*, Cambridge University Press, Cambridge, 2001.
- [19] B. B. Averbeck, P. E. Latham, and A. Pouget, *Neural correlations, population coding and computation*, Nat. Rev. Neurosci. **7**, 358 (2006).
- [20] T. Gawne and B. Richmond, *How independent are the messages carried by adjacent inferior temporal cortical neurons?*, Journal of Neuroscience **13**, 2758 (1993).
- [21] M. R. Cohen and A. Kohn, *Measuring and interpreting neuronal correlations*, Nature Neuroscience **14**, 811 (2011).
- [22] E. Zohary, M. N. Shadlen, and W. T. Newsome, *Correlated neuronal discharge rate and its implications for psychophysical performance.*, Nature **370**, 140 (1994).
- [23] H. Sompolinsky, H. Yoon, K. Kang, and M. Shamir, *Population coding in neuronal systems with correlated noise*, Physical Review E **64**, 051904 (2001).
- [24] L. F. Abbott and P. Dayan, *The effect of correlated variability on the accuracy of a population code.*, Neural Computation **11**, 91 (1999).
- [25] I. Ginzburg and H. Sompolinsky, *Theory of correlations in stochastic neural networks*, Phys. Rev. E. **50**, 3171 (1994).
- [26] T. Sejnowski, *On the stochastic dynamics of neuronal interaction*, Biol. Cybern. **22**, 203 (1976).
- [27] J. Trousdale, Y. Hu, E. Shea-Brown, and K. Josić, *Impact of Network Structure and Cellular Response on Spike Time Correlations*, PLoS. Comput. Biol. **8**, e1002408 (2012).
- [28] Y. Hu, J. Trousdale, K. Josić, and E. Shea-Brown, *Motif Statistics and Spike Correlations in Neuronal Networks*, J. Stat. Mech. **P03012** (2013).
- [29] C. W. Gardiner, *Handbook of Stochastic Methods for Physics, Chemistry and the Natural Sciences*, Springer-Verlag, Berlin, 2009.
- [30] A. G. Hawkes, *Point spectra of some mutually exciting point processes*, J. Roy. Statist. Soc. Ser. B. **33**, 438 (1971).
- [31] J. M. Pedraza and A. van Oudenaarden, *Noise propagation in gene networks*, Science (New York, NY) **307**, 1965 (2005).

- [32] R. Tomioka, H. Kimura, T. J Kobayashi, and K. Aihara, *Multivariate analysis of noise in genetic regulatory networks*, J. Theor. Biol. **229**, 501 (2004).
- [33] I. Lestas, J. Paulsson, N. E. Ross, and G. Vinnicombe, *Noise in Gene Regulatory Networks*, IEEE. T. Automat. Contr. **53**, 189 (2008).
- [34] P. B. Warren, S. Tanase-Nicola, and P. R. Wolde, *Exact results for noise power spectra in linear biochemical reaction networks*, arXiv preprint q-bio/0512041 (2005).
- [35] We quantify second order correlations using the cross-covariance functions, defined by $(\mathbf{C}_y(\tau))_{ij} = \mathbf{E}[(y_i(t) - \mathbf{E}[y_i(t)])(y_j(t + \tau) - \mathbf{E}[y_j(t + \tau)])]$.
- [36] Spectral quantities of stochastic processes are technically defined by considering first the transform over a finite window - i.e., $\tilde{y}(\omega) = \int_0^T dt e^{-2\pi i \omega t} (y_i(t) - \mathbf{E}[y_i(t)])$. The spectrum, for instance, is given by $S_y(\omega) = \lim_{T \rightarrow \infty} \frac{1}{T} \mathbf{E}[\tilde{y}\tilde{y}(\omega)]$.
- [37] Y. J. Wang and G. Y. Wong, *Stochastic blockmodels for directed graphs*, J. Am. Statist. Assoc. **82**, 8 (1987).
- [38] J. J. Daudin, F. Picard, and S. Robin, *A mixture model for random graphs*, Stat. Comput. **18**, 173 (2008).
- [39] A. Litwin-Kumar and B. Doiron, *Slow dynamics and high variability in balanced cortical networks with clustered connections*, Nat. Neurosci. (2012).
- [40] B. J. Pettejohn, M. J. Berryman, and M. D. McDonnell, *Methods for generating complex networks with selected structural properties for simulations: a review and tutorial for neuroscientists*, Front. Comput. Neurosci. **5** (2011).
- [41] R. A. Horn and C. R. Johnson, *Matrix Analysis*, Cambridge University Press, 1990.
- [42] K. Rajan and L. F. Abbott, *Eigenvalue spectra of random matrices for neural networks*, Phys Rev Lett **97**, 188104 (2006).
- [43] D. R. Brillinger, *An introduction to polyspectra*, 1964.
- [44] Y. C. Kim and E. Powers, *Digital Bispectral Analysis and Its Applications to Nonlinear Wave Interactions*, Plasma Science, IEEE Transactions on **7**, 120 (1979).
- [45] P. Huber, B. Kleiner, T. Gasser, and G. Dumermuth, *Statistical methods for investigating phase relations in stationary stochastic processes*, Audio and Electroacoustics, IEEE Transactions on **19**, 78 (1971).
- [46] U. Alon, *Network motifs: theory and experimental approaches*, Nat. Rev. Genet. **8**, 450 (2007).

- [47] J.-P. Pfister and W. Gerstner, *Triplets of spikes in a model of spike timing-dependent plasticity*, The Journal of neuroscience : the official journal of the Society for Neuroscience **26**, 9673 (2006).
- [48] J. Zylberberg and E. Shea-Brown, *Input nonlinearities shape beyond-pairwise correlations and improve information transmission by neural populations*, arXiv preprint arXiv:1212.3549 (2012).
- [49] Y. Hu, J. Zylberberg, and E. Shea-Brown, *The sign rule and beyond: Boundary effects, flexibility, and noise correlations in neural population codes*, arXiv preprint q-Bio/1307.3235 (2013).